

## Electronic Supplementary Information

### Kinetically Controlled Ag<sup>+</sup>-Coordinated Chiral Supramolecular Polymerization Accompanying a Helical Inversion

Heekyoung Choi,<sup>a</sup> Sojeong Heo,<sup>a</sup> Seonae Lee,<sup>a</sup> Ka Young Kim,<sup>a</sup> Jong Hyeon Lim,<sup>b</sup> Sung Ho Jung,<sup>c</sup> Shim Sung Lee,<sup>a</sup> Hiroyuki Miyake,<sup>d</sup> Jin Yong Lee,<sup>\*,b</sup> and Jong Hwa Jung<sup>\*,a</sup>

<sup>a</sup>Department of Chemistry and Research Institute of Natural Sciences, Gyeongsang National University, Jinju 52828, Republic of Korea.

<sup>b</sup>Department of Chemistry, SungKyunKwan University, Suwon 16419, Republic of Korea.

<sup>c</sup>Department of Liberal Arts, Gyeongnam National University of Science and Technology (GNTECH), Jinju 52725, Republic of Korea

<sup>d</sup>Department of Chemistry, Graduate School of Science, Osaka City University, Osaka 558-8585, Japan.

\*E-mail: jonghwa@gnu.ac.kr; jinylee@skku.edu

## Table of Contents

### 1. General

1.1 AFM observation .....	S3
1.2 Circular dichroism studies .....	S3
1.3 Linear dichroism studies .....	S3
1.4 DFT calculation .....	S4
1.5 Preparation of silver complexes .....	S4
1.6 Thermodynamic studies .....	S4

### 2. Synthesis and characterization

2.1 Synthesis of compounds <i>D-1</i> and <i>L-1</i> .....	S6
2.2 Synthesis of compounds <i>D-L<sup>1</sup></i> and <i>L-L<sup>1</sup></i> .....	S6
2.3 Synthesis of compound <i>D-L<sup>2</sup></i> .....	S7
2.4 Synthesis of compound <i>D-L<sup>3</sup></i> .....	S8

### 3. Supplementary scheme and figures.

3.1 Scheme S1 .....	S9
3.2 Figs. S1-S48 .....	S10

### 4. Analytical data

4.1 <sup>1</sup> H- and <sup>13</sup> C-NMR spectroscopy .....	S47
4.2 HR ESI-MS spectrometry .....	S53

### 5. Supplementary references .....

S56

## 1. General

The  $^1\text{H}$  and  $^{13}\text{C}$  NMR spectra were taken on a Bruker DRX 300, and mass spectroscopy samples were analyzed on a JEOL JMS-700 mass spectrometer. The highresolution mass spectra (HR MS) were measured by electrospray ionization (ESI) with a microTOF Focus spectrometer from SYNAPT G2 (Waters, U.K.). X-ray diffraction (XRD) pattern was recorded on a Rigaku model Miniflex600 X-ray diffractometer with a  $\text{Cu K}\alpha$  radiation source. A UV-visible spectrophotometer (Thermo Evolution 600) was used to obtain the absorption spectra. IR spectra were obtained for KBr pellets, in the range  $400\text{--}4000\text{ cm}^{-1}$ , with a Shimadzu FTIR 8400S instrument. Dynamic light scattering (DLS) measurements of  $D\text{-L}^1$  in the presence of  $\text{AgNO}_3$  (1.0 and 2.0 equiv.) in the supramolecular polymerization were carried out using a NanoZS (Malvern UK) employing a 532 nm laser at a back scattering angle of  $173^\circ$ . The samples were measured in a 10 mm glass cuvette. A dead time (Time between sample loading and starting of measurement by the machine) of around 60 seconds is present in all measurements.

### 1.1 AFM observation

Atomic force microscope (AFM) imaging was performed by using XE-100 and a PPP-NCHR 10 M cantilever (Park systems). The AFM samples were prepared by spin-coating (1500 rpm) onto freshly cleaved Muscovite Mica, and images were recorded with the AFM operating in noncontact mode in air at RT with resolution of  $1024 \times 1024$  pixels, using moderate scan rates (0.3 Hz).

### 1.2 Circular dichroism studies

The time-dependent CD spectra were recorded on a Jasco J-815 CD spectrophotometer. CD spectra were determined over the range of 190-700 nm using a quartz cell with 0.1 mm path length. Scans were taken at a rate of 100 nm/min with a sampling interval of 1.0 nm and response time of 1s. The scans were acquired for the solution sample directly at room temperature. Anisotropic factors (gCD) of complexes were calculated by the previously reported method.<sup>[1]</sup>

### 1.3 Linear dichroism studies

The Linear dichroism (LD) spectra were recorded on a Jasco J-815 Spectropolarimeter (150-L Type). LD spectra were recorded over the range of 200-500 nm using a quartz cell with a 0.1

mm path length. Scans were taken at a rate of 20 nm/min with a sampling interval of 0.2 nm and a response time of 2 s.

#### 1.4 DFT calculation of complexes and CD spectra

We performed density functional theory (DFT) calculations to optimize the ligands (B3LYP functional + 6-31G basis set). Coordination structures of  $D-L^1$  with  $Ag^+$  were primarily calculated by geometry optimization process using DFT spectra. The circular dichroism (CD) spectra of suggested structural unit of  $(D-L^1)_2Ag^+$ ,  $D-L^1AgNO_3$ , and  $(D-L^1)_3Ag(NO_3)_2$  complexes were obtained by density functional theory (DFT) calculation by Jaguar software package. The CD spectra were calculated by time-dependent DFT (TDDFT) method<sup>[2]</sup> considering excitation up to 200 singlet excited states. These calculations were done using Becke, three-parameter, Lee-Yang-Parr (B3LYP) exchange-correlation functional<sup>[3]</sup> with the pseudopotential (LanL2DZ)<sup>[4]</sup> and 6-31G basis sets for Ag and other atoms respectively. All the calculations were performed with Gaussian 16 suit of programs.<sup>[5]</sup>

#### 1.5 Preparation of silver complexes

Different concentrations (0~2.0 equiv.) of  $Ag^+$  solution were added to the ligands  $D-L^1$ ,  $L-L^1$ ,  $D-L^2$ , or  $D-L^3$  (8 mM) solution in water. Time- and temperature-dependent CD and UV-vis spectra of complexes were measured.

#### 1.6 Thermodynamic studies

The molar fraction of aggregated molecules ( $\alpha_{agg}$ ) at a certain temperature was calculated from the absorption intensity at 334 or 336.5 nm based on Eq. 1, in which  $Abs(agg)$  and  $Abs(mono)$  are the absorption intensities of fully aggregated (at the lowest temperature) and purely monomeric states (at the highest temperature), respectively, and  $Abs(T)$  is the absorption intensity at a given temperature ( $T$ ).<sup>[6]</sup>

$$\alpha_{agg} = 1 - \frac{Abs(agg) - Abs(T)}{Abs(agg) - Abs(mono)} \quad (1)$$

The plot of  $\alpha_{agg}$  versus temperature provides heating curves with-nonsigmoidal (cooperative mechanism) shape, which were fitted using the models proposed by Meijer et al.<sup>[7]</sup> (for cooperative mechanism). The standard values of enthalpy ( $\Delta H^\circ$ ), entropy ( $\Delta S^\circ$ ), and Gibbs free energy ( $\Delta G^\circ$ ) were calculated using the van't Hoff equation.

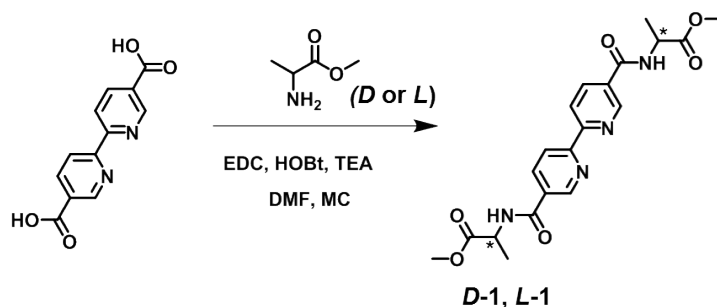
The van't Hoff plots were produced using equation by a method that has been proposed in previous literature.<sup>[8,9]</sup> The values for the entropy change ( $\Delta S$ ) and enthalpy change ( $\Delta H$ ) as used in the cooperative supramolecular polymerization models were obtained by fitting to the

heating or cooling curves. <sup>[10-12]</sup> These heating or cooling curves were obtained by temperature dependent circular dichroism (CD) and UV-vis spectra.

## 2. Synthesis and characterization

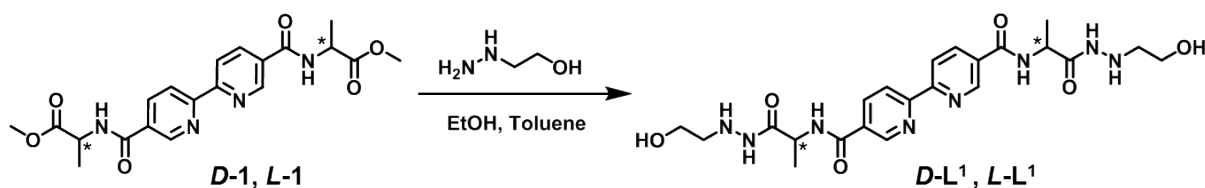
Unless otherwise noted, chemical reagents and solvents were purchased from commercial suppliers (Tokyo Chemical Industry (TCI), Sigma Aldrich) and used without further purification.

### 2.1 Synthesis of compounds *D-1* and *L-1*



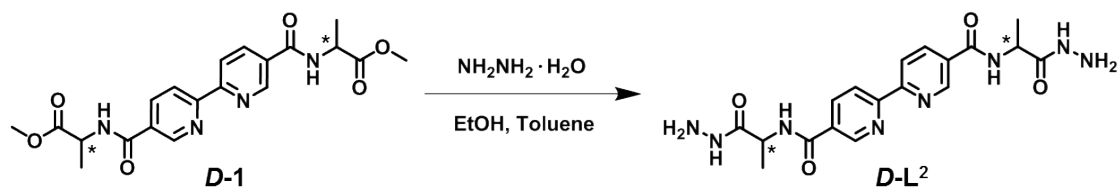
To a mixture of the 2,2'-bipyridine-5,5'-dicarboxylic acid (1.0 g, 4.1 mmol), *D*- or *L*-alanine methyl ester hydrochloride (1.20 g, 8.6 mmol), HOBt·H<sub>2</sub>O (1.11 g, 8.2 mmol) and EDC·HCl (2.36 g, 12.3 mmol) in CH<sub>2</sub>Cl<sub>2</sub>/DMF (4:1, 25 mL) was added TEA 3.4 mL at 0 °C. The reaction mixture was stirred for 1 h and was heated up to room temperature. After stirring for 2 days at room temperature, the mixture was extracted with CH<sub>2</sub>Cl<sub>2</sub> (3 x 30 mL). The combined organics were washed with brine, dried (Na<sub>2</sub>SO<sub>4</sub>), and concentrated. The resulting crude product was purified by recrystallization from CH<sub>2</sub>Cl<sub>2</sub>/ether to give a white solid, compound *D-1* and *L-1* (0.99 g, 58% for *D-1* and 1.02 g, 60% for *L-1*). Decomposition 260 °C; IR (KBr pellet): 3319, 3049, 2997, 2955, 1736, 1635, 1592, 1526, 1460, 1321, 1279, 1241, 1216, 1168 cm<sup>-1</sup>; <sup>1</sup>H NMR (300 MHz, DMSO-*d*<sub>6</sub>) δ= 9.27 – 9.02 (m, 4H), 8.63 – 8.51 (m, 2H), 8.43 (dd, *J* = 8.3, 2.2 Hz, 2H), 4.55 (p, *J* = 7.3 Hz, 2H), 3.68 (s, 6H), 1.45 (d, *J* = 7.3 Hz, 6H); <sup>13</sup>C NMR (75 MHz, DMSO-*d*<sub>6</sub>) δ= 173.41, 164.99, 156.97, 149.16, 137.05, 130.01, 121.08, 52.47, 48.83, 17.18; HRMS (ESI-TOF, positive mode, MeOH/H<sub>2</sub>O 1:1): *m/z* calculated for C<sub>20</sub>H<sub>22</sub>N<sub>4</sub>O<sub>6</sub> [M+H]<sup>+</sup>: 415.1618, found: 415.1618

### 2.2 Synthesis of compounds *D-L*<sup>1</sup> and *L-L*<sup>1</sup>



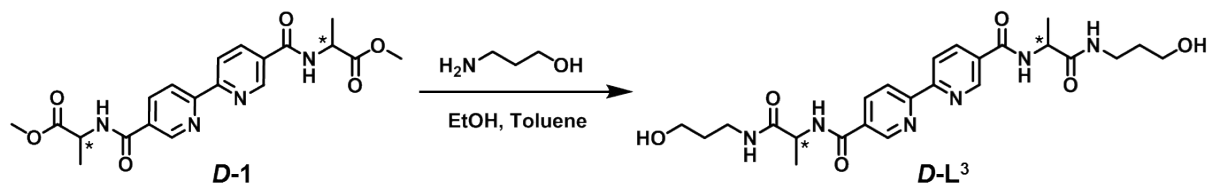
A mixture of compound **D-1** or **L-1** (0.5 g, 1.2 mmol) and 2-hydroxyethylhydrazine (0.33 mL, 4.8 mmol) in a solution of ethanol (20 mL) and toluene (5 mL) was heated at 120 °C for 48 h. The precipitate was filtered, washed with CH<sub>2</sub>Cl<sub>2</sub>, ethanol, diethyl ether and dried in vacuo to give solid product. Finally, the desired products were purified by recrystallization in CH<sub>2</sub>Cl<sub>2</sub>/ether to give white solid, compound **D-L<sup>1</sup>** and **L-L<sup>1</sup>** (0.47 g, 78% for **D-L<sup>1</sup>** and 0.49g, 80% for **L-L<sup>1</sup>**). mp. 231-236 °C; IR (KBr pellet): 3377, 3270, 1655, 1594, 1544, 1461, 1368, 1327, 1276, 1241, 1222 cm<sup>-1</sup>; <sup>1</sup>H NMR (300 MHz, DMSO-*d*<sub>6</sub>) δ= 9.52 (d, *J* = 0.6 Hz, 2H), 9.17 (dd, *J* = 2.2, 0.8 Hz, 2H), 8.88 (d, *J* = 7.4 Hz, 2H), 8.54 (dd, *J* = 8.3, 0.6 Hz, 2H), 8.44 (dd, *J* = 8.3, 2.2 Hz, 2H), 4.99(brs, 2H), 4.50(s, 4H), 3.44 (q, *J* = 5.7 Hz, 4H), 2.75(s, 4H), 1.38 (d, *J* = 7.2 Hz, 6H); <sup>13</sup>C NMR (75 MHz, DMSO-*d*<sub>6</sub>) δ= 171.36, 164.85, 156.80, 149.31, 137.17, 130.40, 120.87, 59.19, 53.95, 48.41, 18.42; HRMS (ESI-TOF, positive mode, MeOH/H<sub>2</sub>O 1:1): *m/z* calculated for C<sub>22</sub>H<sub>30</sub>N<sub>8</sub>O<sub>6</sub> [M+H]<sup>+</sup>: 503.2367, found: 503.2365

### 2.3 Synthesis of compound **D-L<sup>2</sup>**



A mixture of compound **D-1** (0.5 g, 1.2 mmol) and hydrazine hydrate (0.15 mL, 4.8 mmol) in a solution of ethanol (20 mL) and toluene (5 mL) was heated at 120 °C for 30 h. The precipitate was filtered, washed with dimethylene chloride to remove unreacted starting material, and dried in vacuo to give solid product. Finally, the product was purified by recrystallization in CH<sub>2</sub>Cl<sub>2</sub> to give white solid (0.45g, 90% yield). Decomposition 285 °C; IR (KBr pellet): 3285, 3050, 1651, 1593, 1526, 1462, 1271, 1187 cm<sup>-1</sup>; <sup>1</sup>H NMR (300 MHz, DMSO-*d*<sub>6</sub>) δ= 9.33 – 9.10 (m, 4H), 8.86 (d, *J* = 7.5 Hz, 2H), 8.55 – 8.39 (m, 4H), 4.51 (p, *J* = 7.1 Hz, 2H), 4.28(s, 4H), 1.36 (d, *J* = 7.2 Hz, 6H); <sup>13</sup>C NMR (75 MHz, DMSO-*d*<sub>6</sub>) δ= 171.92, 164.79, 156.77, 149.31, 137.15, 130.43, 120.84, 48.32, 18.54; HRMS (ESI-TOF, positive mode, MeOH/H<sub>2</sub>O 1:1): *m/z* calculated for C<sub>18</sub>H<sub>22</sub>N<sub>8</sub>O<sub>4</sub> [M+H]<sup>+</sup>: 415.1842, found: 415.1840

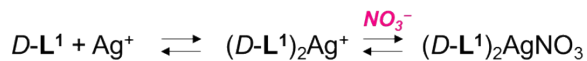
## 2.4 Synthesis of compound *D-L*<sup>3</sup>



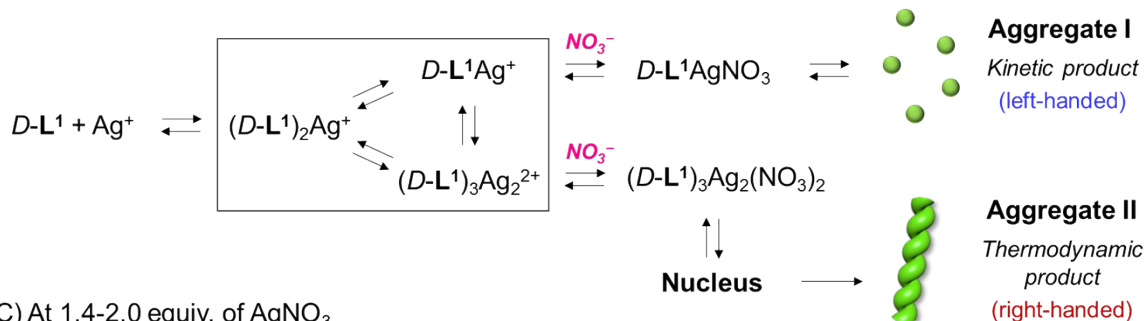
A mixture of compound **D-1** (0.5 g, 1.2 mmol) and 3-amino-1-propanol (0.37 mL, 4.8 mmol) in a solution of ethanol (20 mL) and toluene (5 mL) was heated at 120 °C for 48 h. The precipitate was filtered, washed with CH<sub>2</sub>Cl<sub>2</sub>, ethanol, diethyl ether and dried in vacuo to give the solid. The precipitate was filtered, washed with CH<sub>2</sub>Cl<sub>2</sub>, ethanol, diethyl ether and dried in vacuo to give solid product. Finally, the precipitate was purified by recrystallization from CH<sub>2</sub>Cl<sub>2</sub>/ether, to give solid 0.47 g, 78% yield). Decomposition 295 °C; IR (KBr pellet): 3359, 3292, 3100, 2936, 2873, 1641, 1593, 1527, 1459, 1248, 1186 cm<sup>-1</sup>; <sup>1</sup>H NMR (300 MHz, DMSO-*d*<sub>6</sub>) δ= 9.18 (dd, *J* = 2.1, 0.7 Hz, 2H), 8.85 (d, *J* = 7.4 Hz, 2H), 8.66 – 8.32 (m, 4H), 7.98 (t, *J* = 5.6 Hz, 2H), 4.65 – 4.27 (m, 4H), 3.57 – 3.37 (m, 4H), 3.30 – 2.96 (m, 3H), 1.58 (p, *J* = 6.6 Hz, 4H), 1.37 (d, *J* = 7.2 Hz, 6H); <sup>13</sup>C NMR (75 MHz, DMSO-*d*<sub>6</sub>) δ= 172.47, 164.79, 156.80, 149.29, 137.14, 130.47, 120.88, 58.93, 49.57, 36.40, 32.80, 18.50; HRMS (ESI-TOF, positive mode, MeOH/H<sub>2</sub>O 1:1): *m/z* calculated for C<sub>24</sub>H<sub>32</sub>N<sub>6</sub>O<sub>6</sub> [M+H]<sup>+</sup>: 501.2462, found: 501.2458

### 3. Supplementary scheme and figures

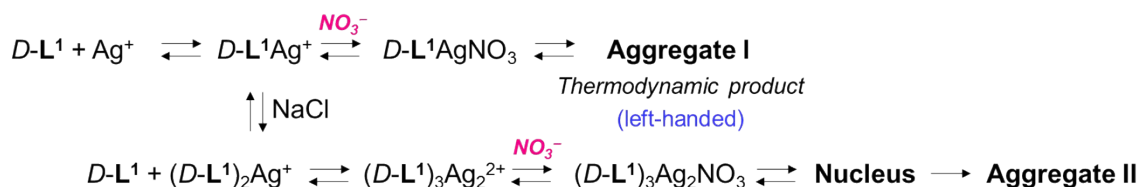
(A) At less than 0.4 equiv. of  $\text{AgNO}_3$



(B) At 0.5-1.3 equiv. of  $\text{AgNO}_3$



(C) At 1.4-2.0 equiv. of  $\text{AgNO}_3$



**Scheme S1.** The formation mechanism of aggregates based on  $D\text{-L}^1$  at different concentration of  $\text{AgNO}_3$ ; (A) formation of  $(D\text{-L}^1)_2\text{AgNO}_3$ , (B) the aggregate II based on  $(D\text{-L}^1)_3\text{Ag}_2(\text{NO}_3)_2$ , and (C) the aggregate I based on  $D\text{-L}^1\text{AgNO}_3$ .

**ESI-MS Study:** When 0.4 equiv. of  $\text{AgNO}_3$  was added to ligand  $D\text{-L}^1$  (8 mM), a peak for the  $[(D\text{-L}^1)_2\text{Ag}]^+$  complex was observed at  $m/z$  1113.3651 according to high-resolution electron spray ionization mass spectroscopy (HR ESI-MS) (Fig. S1), which is indicative of 2:1 ( $D\text{-L}^1\text{:Ag}^+$ ) complex formation. In contrast, peaks for  $[(D\text{-L}^1)_2\text{Ag}]^+$ ,  $[(D\text{-L}^1)_3\text{Ag}_2]^{2+}$ , and  $[D\text{-L}^1\text{Ag}]^+$  complexes were observed at  $m/z$  1113.3651, 861.2487, and 611.1343 at a 1.3:1:1.3 ratio in the presence of 1.0 equiv. of  $\text{Ag}^+$ , indicating 2:1, 3:2, and 1:1 complexes, respectively (Fig. S2 and Scheme S1). These findings demonstrate that a mixture of 2:1, 1:1, and 3:2 ( $D\text{-L}^1\text{:Ag}^+$ ) complexes is formed in the presence of 1.0 equiv. of  $\text{Ag}^+$ .

More interestingly, upon aging for 240 min, the transparent solution transforms into a colloidal suspension (Fig. S3A). The colloidal particles were isolated to obtain information on the complex structure therein. A new peak was observed at  $m/z$  1784.4379 in the ESI/TOF-MS trace (Fig. S3B), which corresponds to  $[(D\text{-L}^1)_3\text{Ag}_2\text{NO}_3]^+$  (Scheme S1). The peak for  $[(D\text{-L}^1)_3\text{Ag}_2\text{NO}_3]^+$  was obtained by fragmentation of  $[(D\text{-L}^1)_3\text{Ag}_2(\text{NO}_3)_2]$ . At 2.0 equiv. of  $\text{AgNO}_3$ , a major peak was obtained at  $m/z$  611.1343 corresponding to  $[D\text{-L}^1\text{Ag}]^+$  after aging for 30 min (Fig. S4). This peak was obtained by fragmentation of  $D\text{-L}^1\text{AgNO}_3$ , implying that  $D\text{-L}^1$  forms a 1:1 complex with excess  $\text{Ag}^+$ . Additionally, a peak for  $[(D\text{-L}^1)_2\text{Ag}_2\text{NO}_3]^+$  was obtained at  $m/z$  1282.2551.

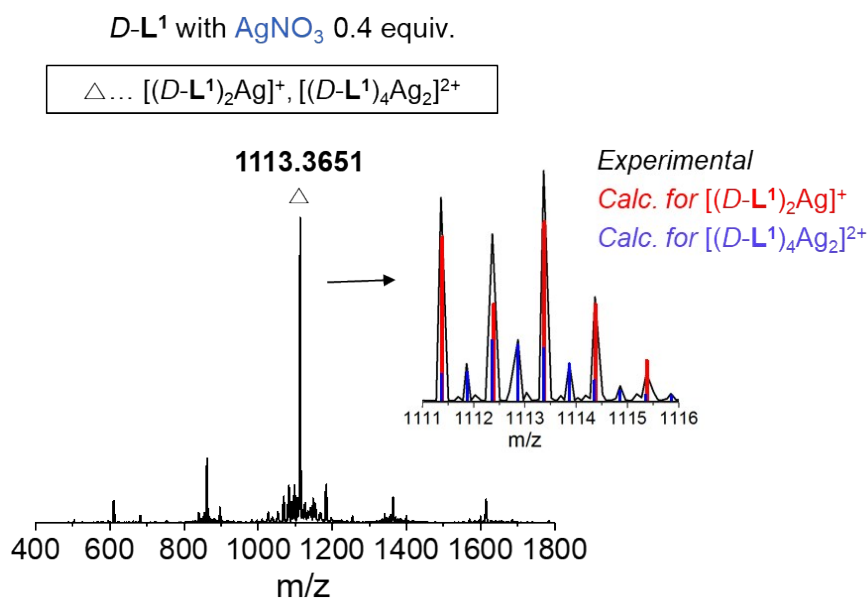


**Fig. S1** HR ESI-MS spectrum of  $D\text{-L}^1$  with  $\text{AgNO}_3$  (0.4 equiv.) in water.

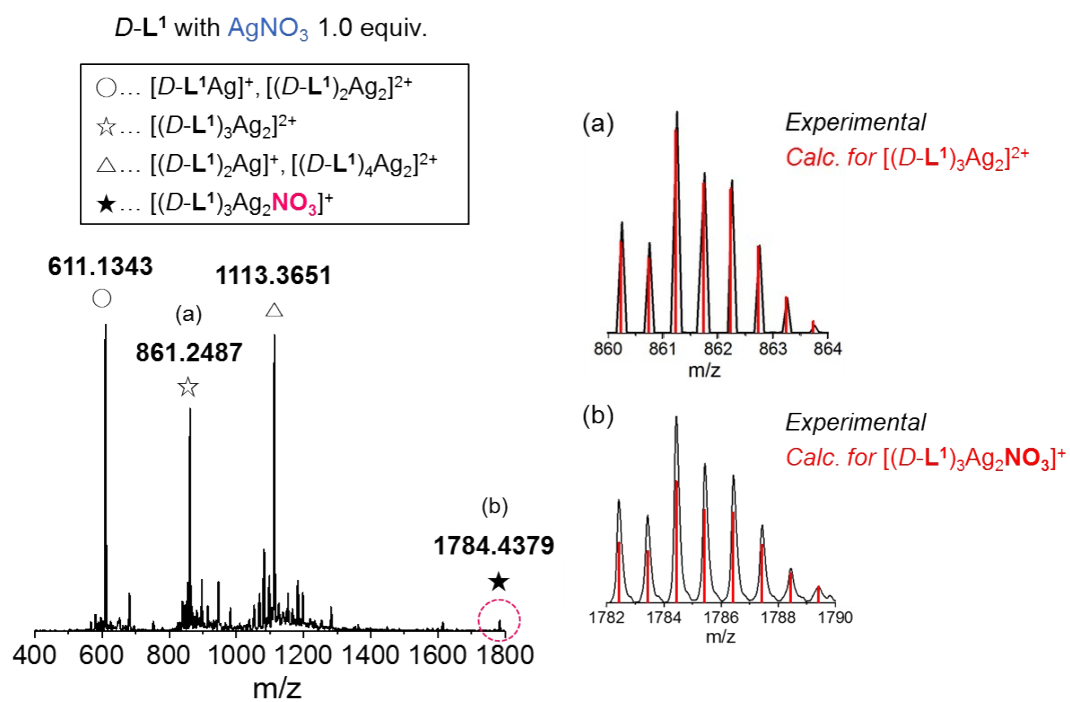


**Fig. S2** HR ESI-MS spectrum of  $D-L^1$  with  $AgNO_3$  (1.0 equiv.) in water.

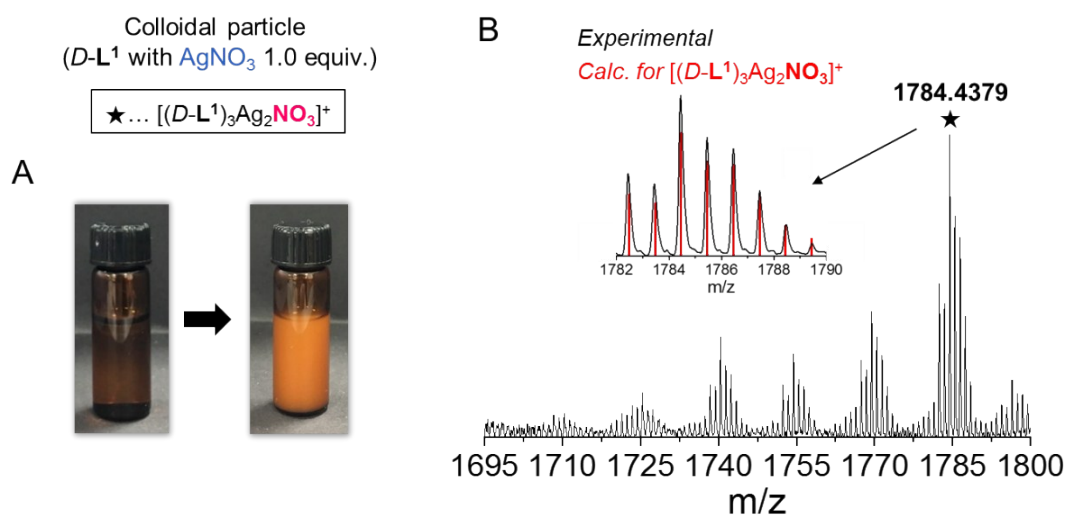


**Fig. S3** (A) Photograph of *D-L*<sup>1</sup> with AgNO<sub>3</sub> (1.0 equiv.) after aging for 10 min (left: transparent solution) and 240 min (right: colloidal solution). (B) HR ESI/TOF-MS spectrum of the colloidal particle separated in mixed *D-L*<sup>1</sup> (8 mM) with AgNO<sub>3</sub> (1.0 equiv.) in water.

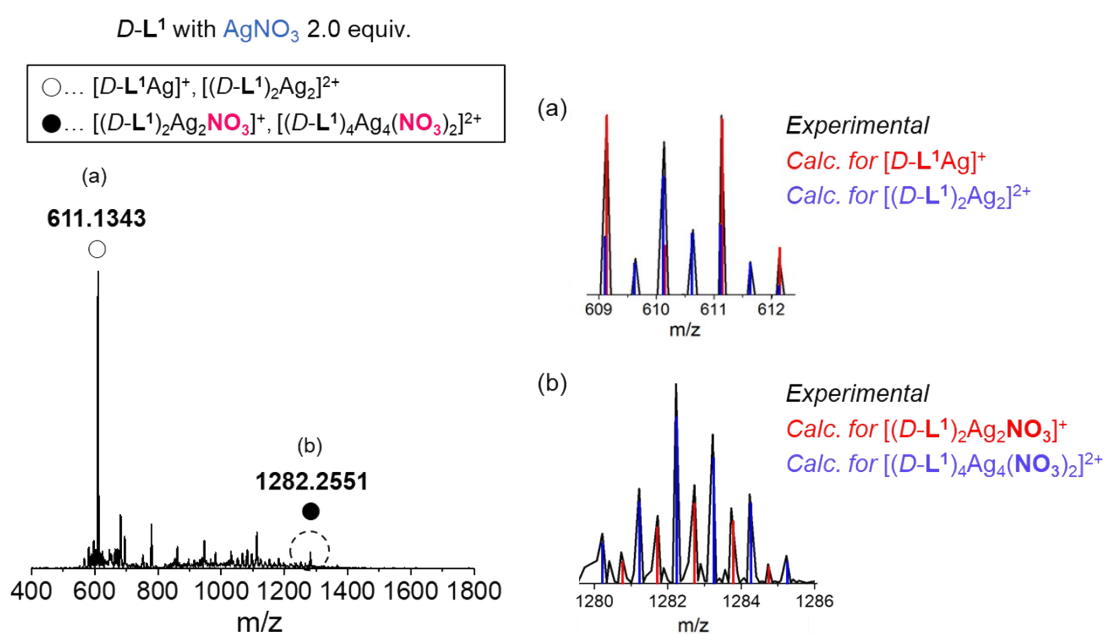


**Fig. S4** HR ESI-MS spectrum of *D-L*<sup>1</sup> with AgNO<sub>3</sub> (2.0 equiv.) in water.

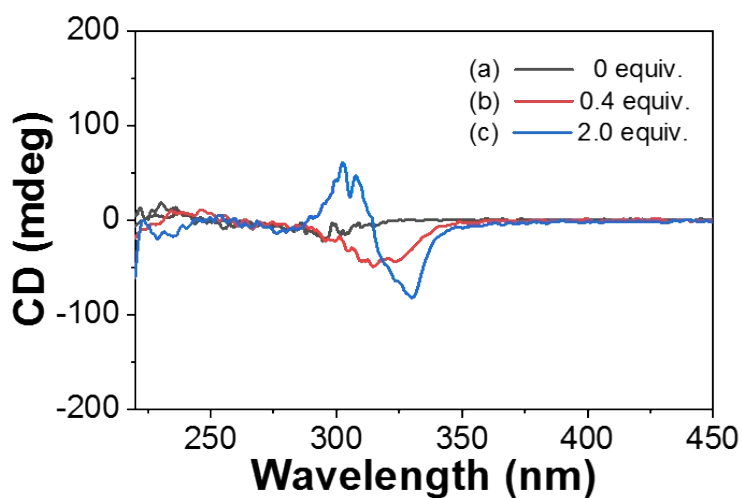


**Fig. S5** CD spectra of *D-L*<sup>1</sup> (8 mM) (a) without and with  $\text{AgNO}_3$  (b) 0.4 and (c) 2.0 equiv. in water.

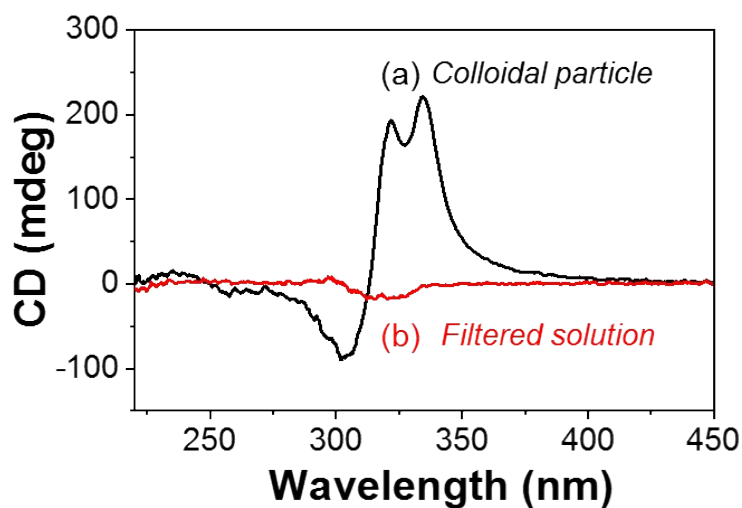


**Fig. S6** CD spectra of (a) the colloidal particle (the aggregate II) and (b) solution separated from the colloidal solution produced in mixed *D-L*<sup>1</sup> (8 mM) with  $\text{AgNO}_3$  (1.0 equiv.) in water.

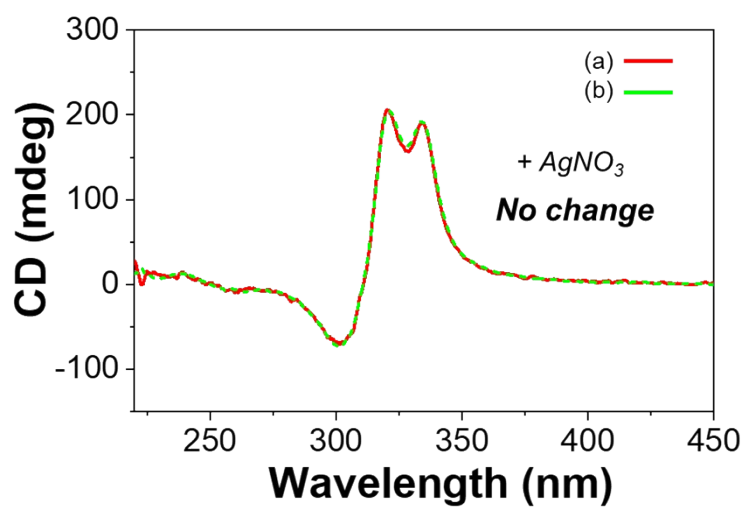


**Fig. S7** CD spectra obtained before (a: red line) and after (b: green line) addition of  $\text{AgNO}_3$  (1.0 equiv.) to the aggregate II (supramolecular polymer) based on  $(D\text{-L}^1)_3\text{Ag}_2(\text{NO}_3)_2$  in water.

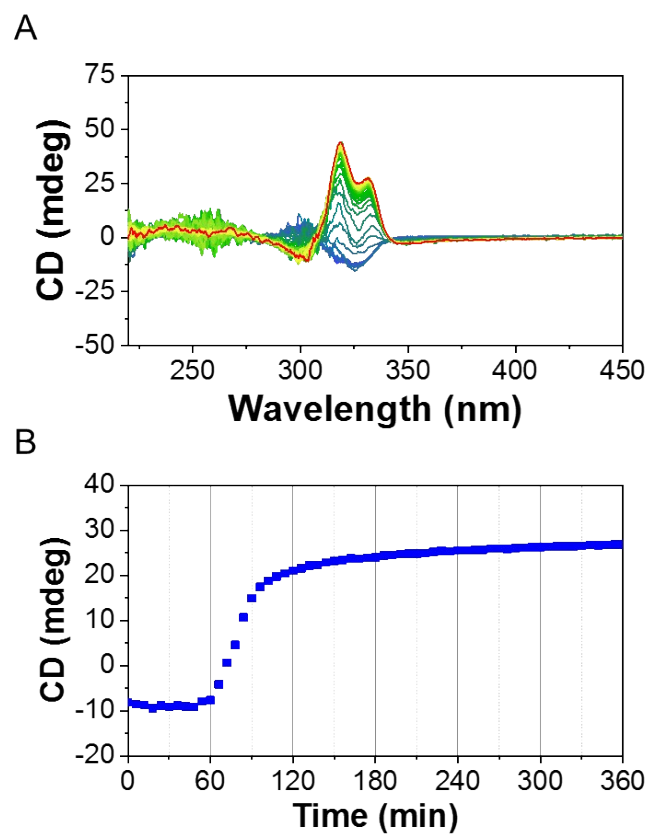


**Fig. S8** (A) Time-dependent CD spectra of *D-L*<sup>1</sup> (8 mM) with  $\text{AgNO}_3$  (1.3 equiv.) in water. (B) Plot for CD spectra changes of *D-L*<sup>1</sup> vs time in the presence of  $\text{AgNO}_3$  (1.3 equiv.) at 334 nm in water.

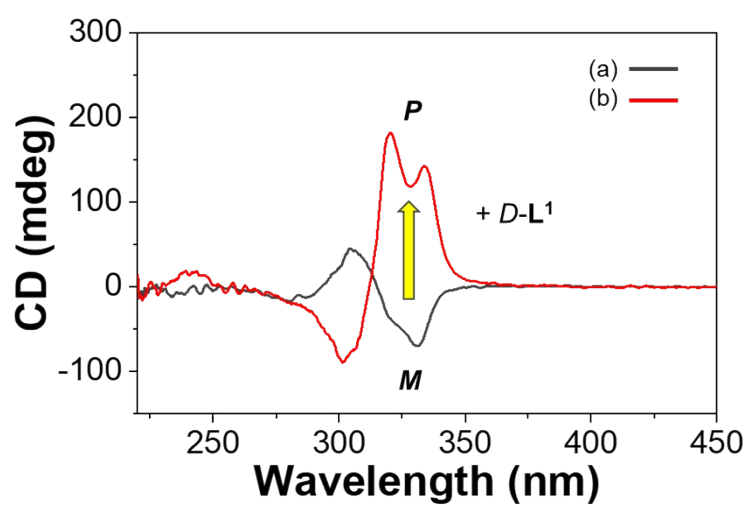


**Fig. S9** CD spectra obtained (a) before and (b) after addition of free ligand  $D-L^1$  (0.5 equiv.) to the aggregate I based on the  $D-L^1AgNO_3$  complex formed in the presence of  $D-L^1$  (8 mM) and  $AgNO_3$  (1.5 equiv.) in water.

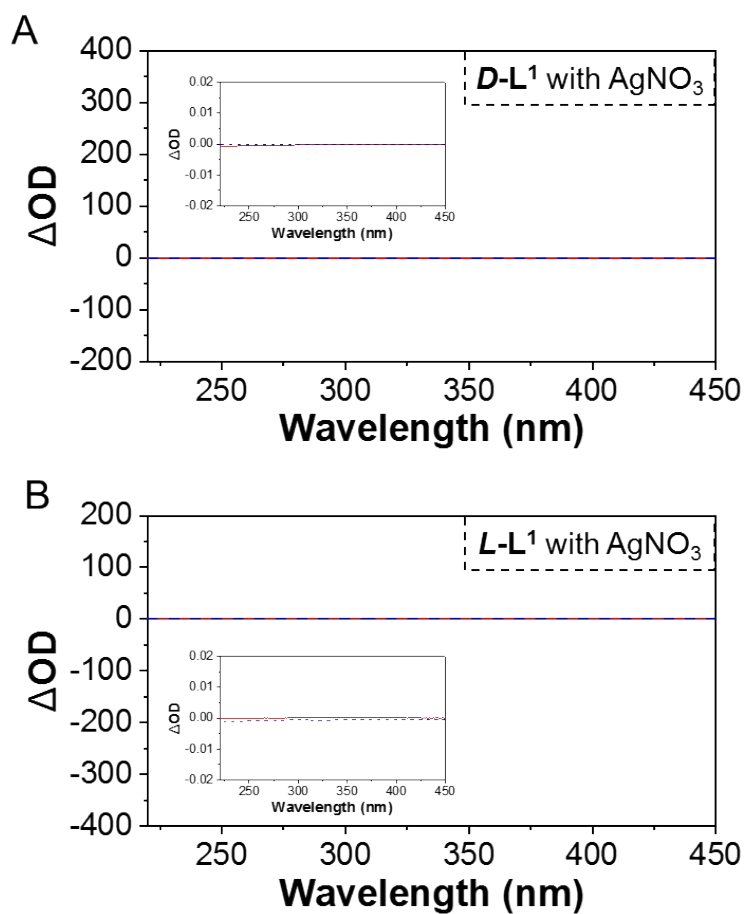


**Fig. S10** LD spectra of (A) *D-L*<sup>1</sup> (8 mM), and (B) *L-L*<sup>1</sup> (8 mM) with 1.0 (red line), and 1.4 (blue dashed line) equiv. of AgNO<sub>3</sub> in water after 3 h.

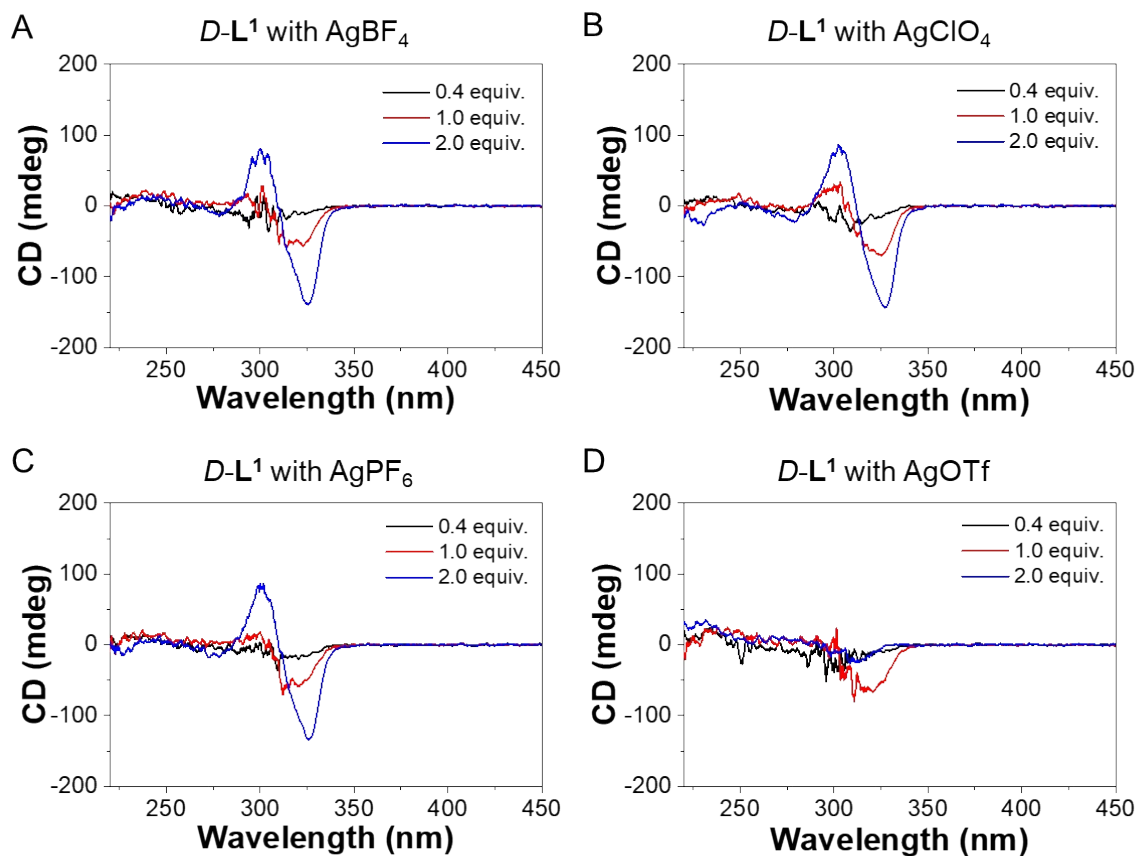


**Fig. S11** CD spectra of *D-L*<sup>1</sup> (8 mM) upon addition of different concentrations (0.4, 1.0, and 2.0 equiv.) of (A) AgBF<sub>4</sub>, (B) AgClO<sub>4</sub>, (C) AgPF<sub>6</sub>, and (D) AgOTf in water.

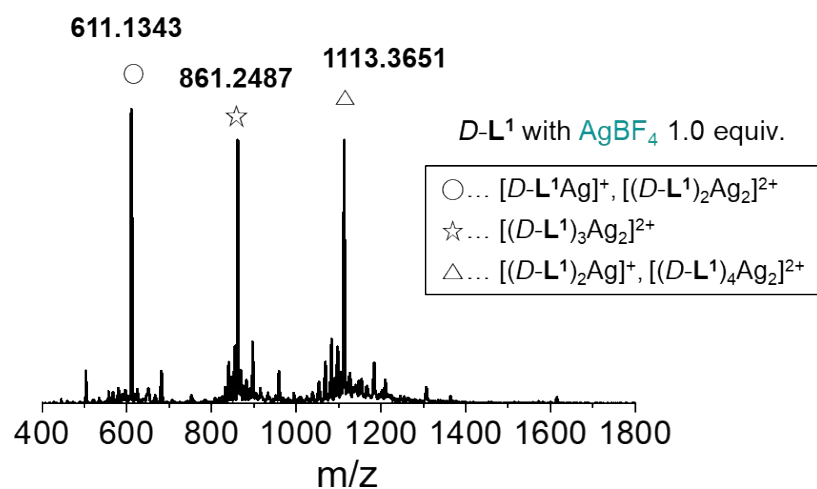


**Fig. S12** HR ESI-MS spectrum of *D-L*<sup>1</sup> (8 mM) with  $\text{AgBF}_4$  (1.0 equiv.) in water.

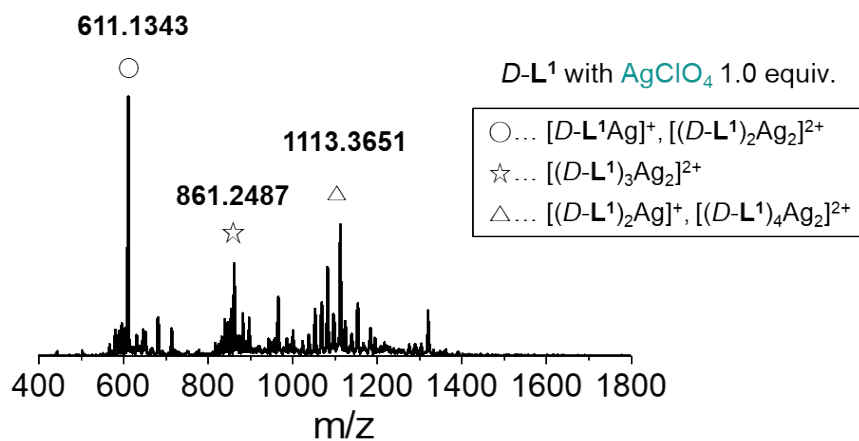


**Fig. S13** HR ESI-MS spectrum of *D-L*<sup>1</sup> (8 mM) with  $\text{AgClO}_4$  (1.0 equiv.) in water.

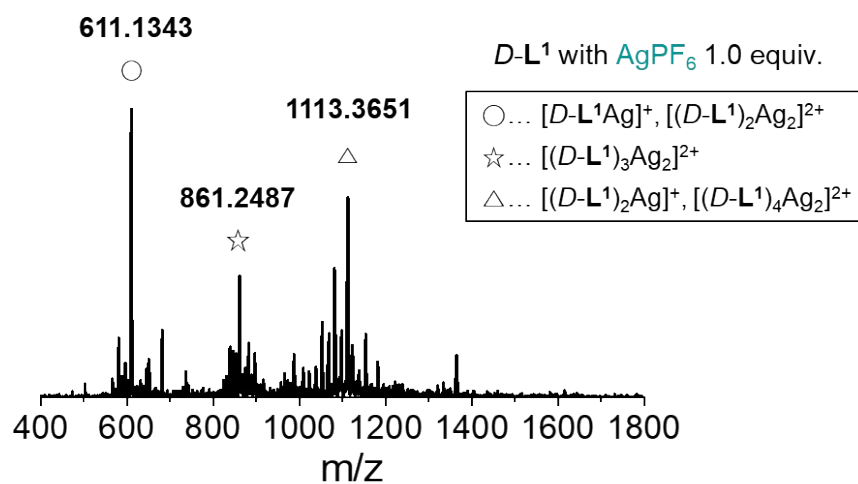


**Fig. S14** HR ESI-MS spectrum of *D-L<sup>1</sup>* (8 mM) with AgPF<sub>6</sub> (1.0 equiv.) in water.

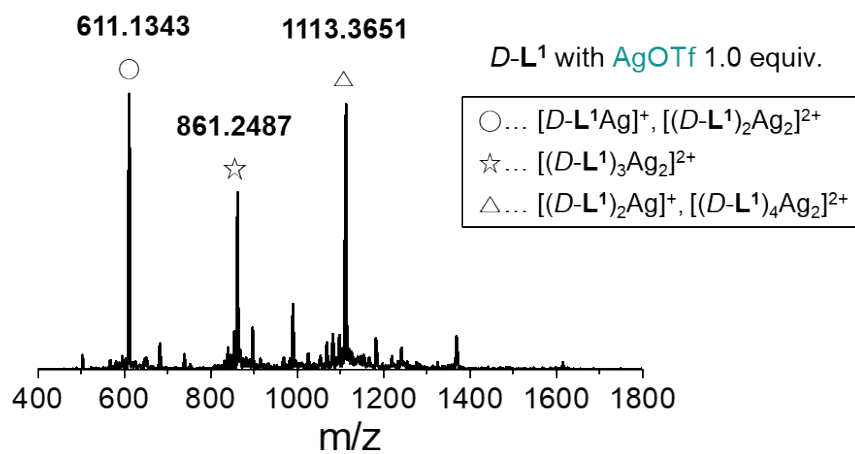


**Fig. S15** HR ESI-MS spectrum of *D-L<sup>1</sup>* (8 mM) with AgOTf (1.0 equiv.) in water.

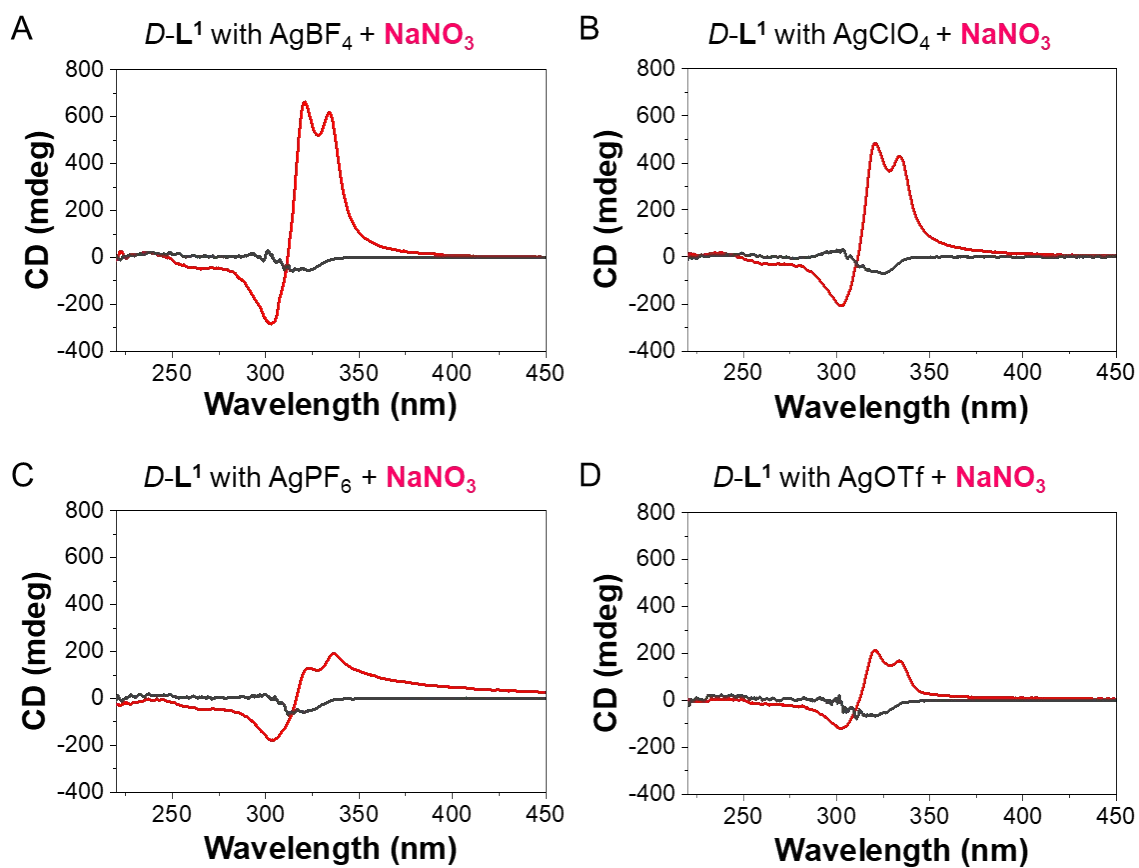


**Fig. S16** CD spectra of  $D\text{-L}^1$  (8 mM) upon addition of  $\text{NaNO}_3$  (2.0 equiv.) in the presence of (A)  $\text{AgBF}_4$  (1.0 equiv.), (B)  $\text{AgClO}_4$  (1.0 equiv.), (C)  $\text{AgPF}_6$  (1.0 equiv.), and (D)  $\text{AgOTf}$  (1.0 equiv.) in water; black line =  $D\text{-L}^1 + \text{Ag}^+$  (1.0 equiv.), red line =  $D\text{-L}^1 + \text{Ag}^+$  (1.0 equiv.) +  $\text{NaNO}_3$  (2.0 equiv.).

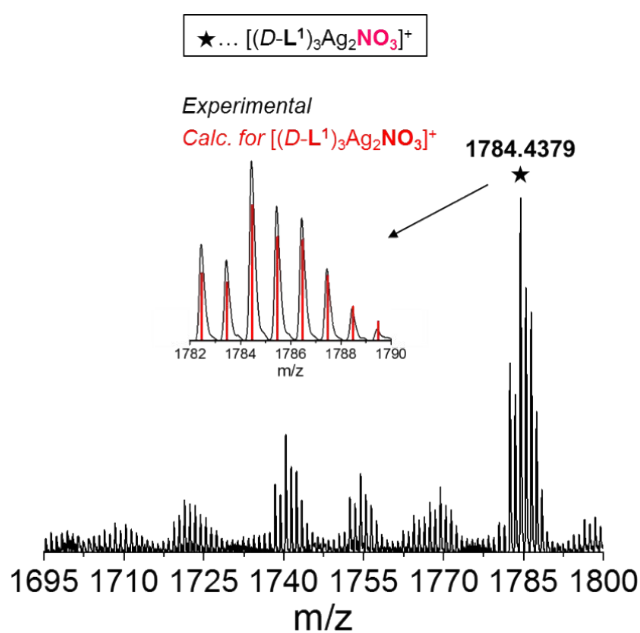


**Fig. S17** HR ESI/TOF-MS spectrum of  $D-L^1$  (8 mM) upon addition of  $NaNO_3$  (2.0 equiv.) in the presence of  $AgOTf$  (1.0 equiv.) in water. The peaks at  $m/z = 611.1343$ ,  $861.2487$  and  $1113.3651$  were obtained by fragment of  $[(D-L^1)_3Ag_2NO_3]^+$  ( $m/z = 1784.4379$ ).

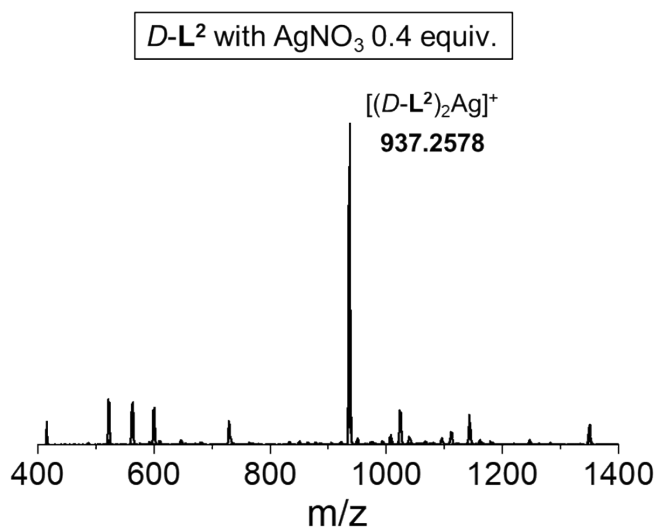


**Fig. S18** HR ESI-MS spectrum of  $D-L^2$  (8 mM) with 0.4 equiv. of  $AgNO_3$  in water.

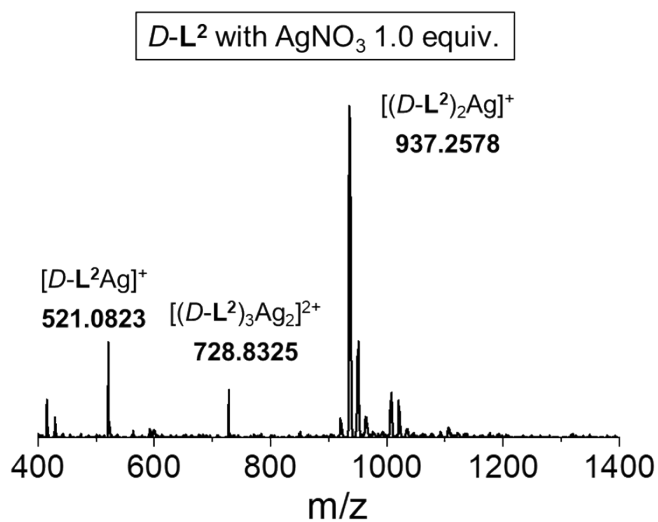


**Fig. S19** HR ESI-MS spectrum of  $D-L^2$  (8 mM) with 1.0 equiv. of  $AgNO_3$  in water.

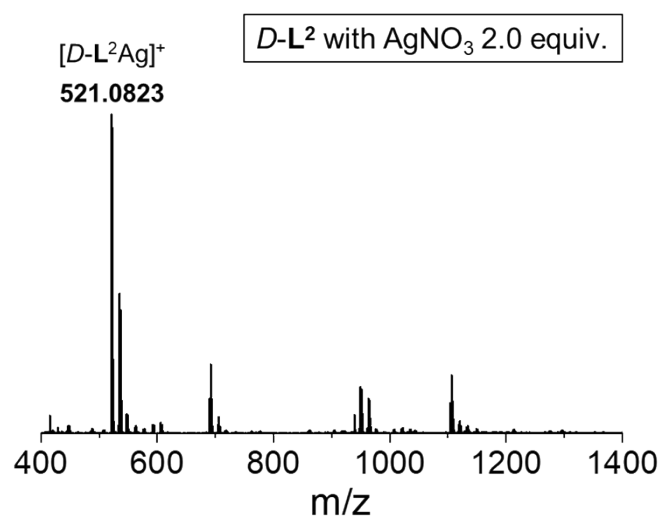


**Fig. S20** HR ESI-MS spectrum of  $D-L^2$  (8 mM) with 2.0 equiv. of  $AgNO_3$  in water.

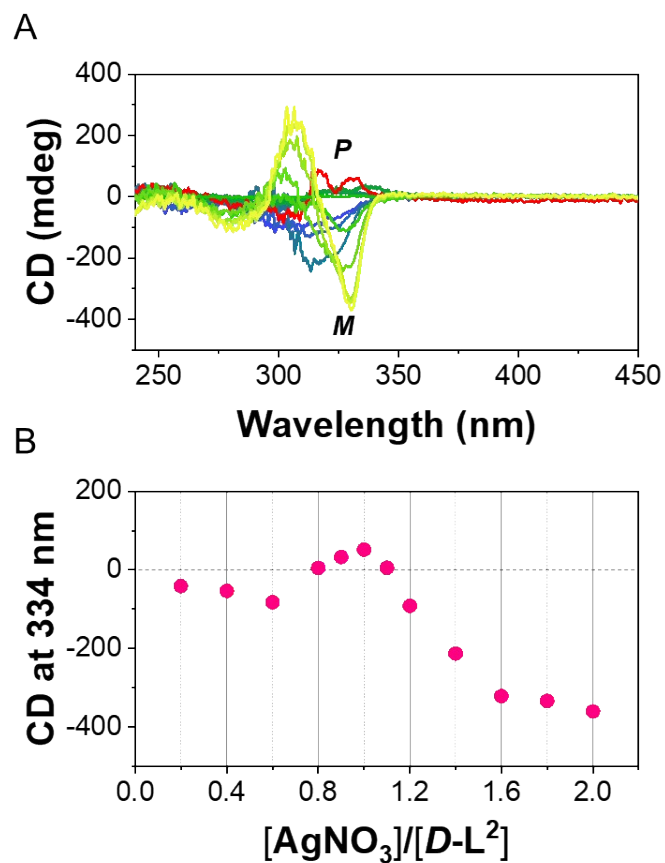


**Fig. S21** (A) CD spectra of  $D-L^2$  (8 mM) upon addition of  $AgNO_3$  in water. (B) Plot for the CD intensity at 334 nm against the equivalents of  $AgNO_3$ .

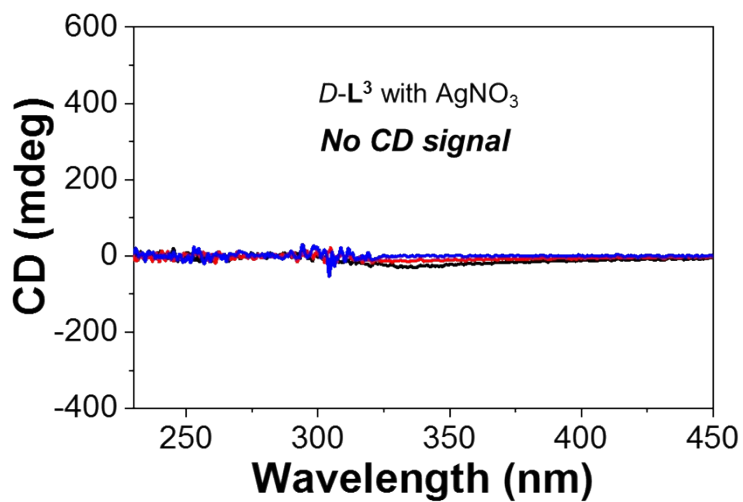


**Fig. S22** CD spectra of  $D-L^3$  (8 mM) with 0.4 (black line), 1.0 (red line), and 2.0 (blue line) equiv. of  $AgNO_3$  in water after 1 day.

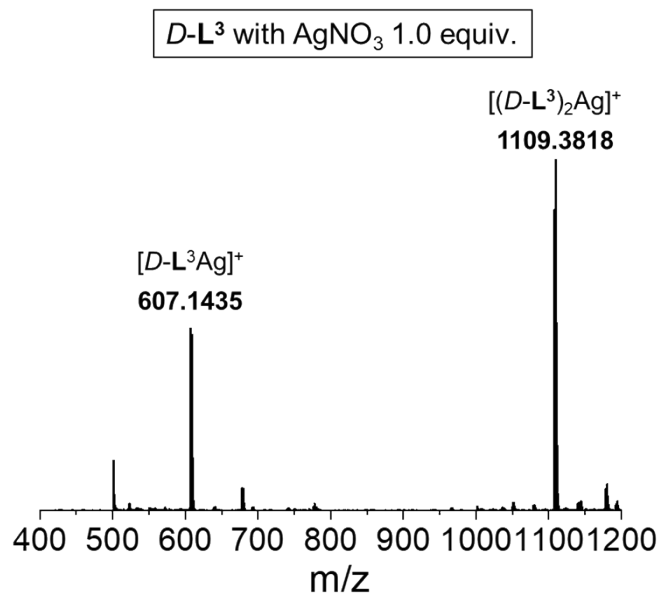


**Fig. S23** HR ESI-MS spectrum of  $D-L^3$  (8 mM) with 1.0 equiv. of  $AgNO_3$  in water.

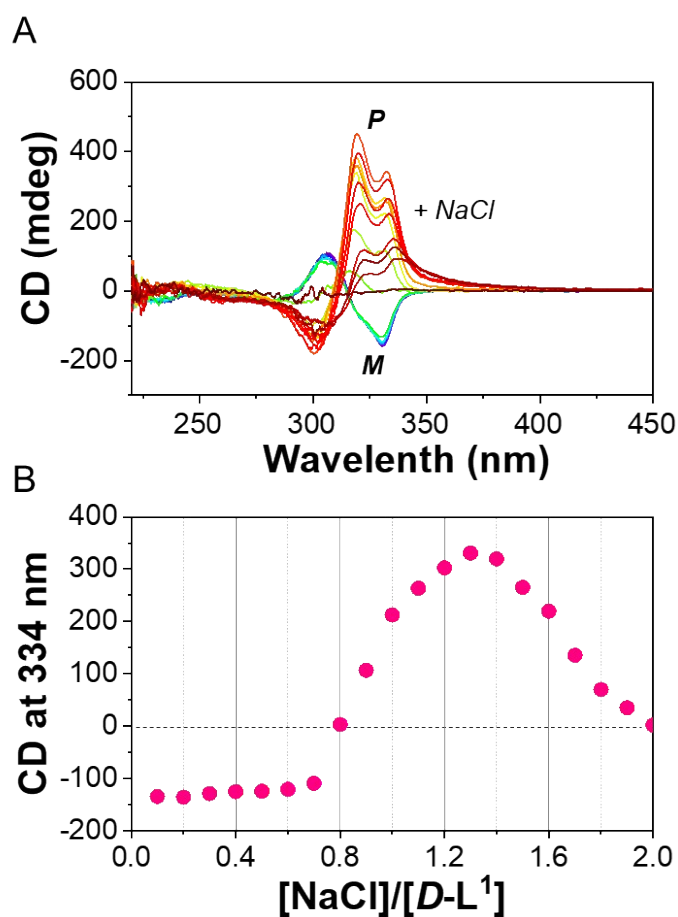


**Fig. S24** (A) CD spectra obtained upon addition of NaCl (0-2.0 equiv.) to the aggregate I based on  $D\text{-L}^1\text{AgNO}_3$  complex produced from a mixed  $D\text{-L}^1$  (8 mM) and  $\text{AgNO}_3$  (2.0 equiv.) in water. (B) Plot for the CD intensity against the equivalents of NaCl.

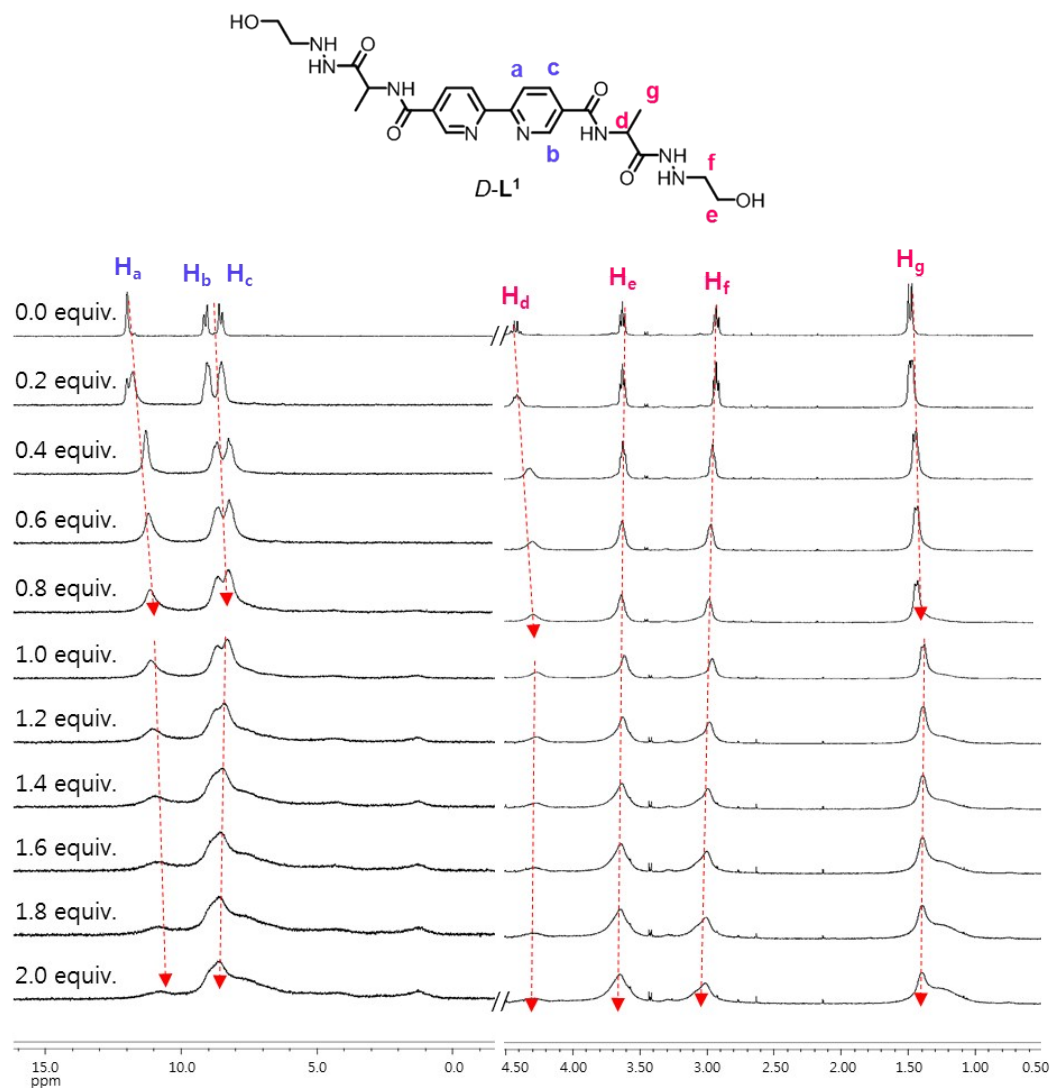
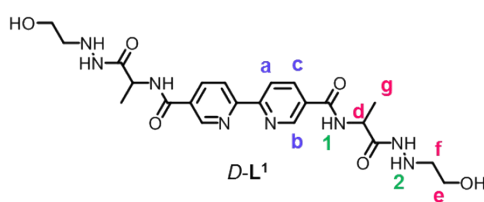


**Fig. S25**  $^1\text{H-NMR}$  spectra of  $D\text{-L}^1$  upon addition of  $\text{AgNO}_3$  (0-2.0 equiv.) in  $\text{D}_2\text{O}$  and  $\text{H}_2\text{O}$  (1:1 v/v).

**Additional Explanation;** The aromatic protons ( $\text{H}_a$ ,  $\text{H}_b$ , and  $\text{H}_c$ ) of  $D\text{-L}^1$  shifted to the high field upon increasing the concentration of  $\text{AgNO}_3$ . The chemical pyridine protons were ca. 5-fold larger than those of the alkyl chain protons. The relatively large chemical shifts of the aromatic protons occurred due to the shielding effect with  $\pi\text{-}\pi$  stacking between  $D\text{-L}^1$  and  $D\text{-L}^1$  via coordination bonds with  $\text{Ag}^+$ . Additionally, the sharp aromatic protons peaks gradually broadened upon addition of  $\text{AgNO}_3$ . These results also suggest that  $\text{AgNO}_3$  was coordinated to ligand  $D\text{-L}^1$ .



MeOD/H <sub>2</sub> O (1:1)	NH (1)	H <sub>a</sub>	NH (2)	H <sub>b</sub>	H <sub>c</sub>
<i>D-L</i> <sup>1</sup>	9.76	9.11	8.96	8.44	8.38
<i>D-L</i> <sup>1</sup> -AgOTf	10.05	8.47	9.06	-	-
$\Delta$ ppm	0.29	-0.64	0.1	-	-

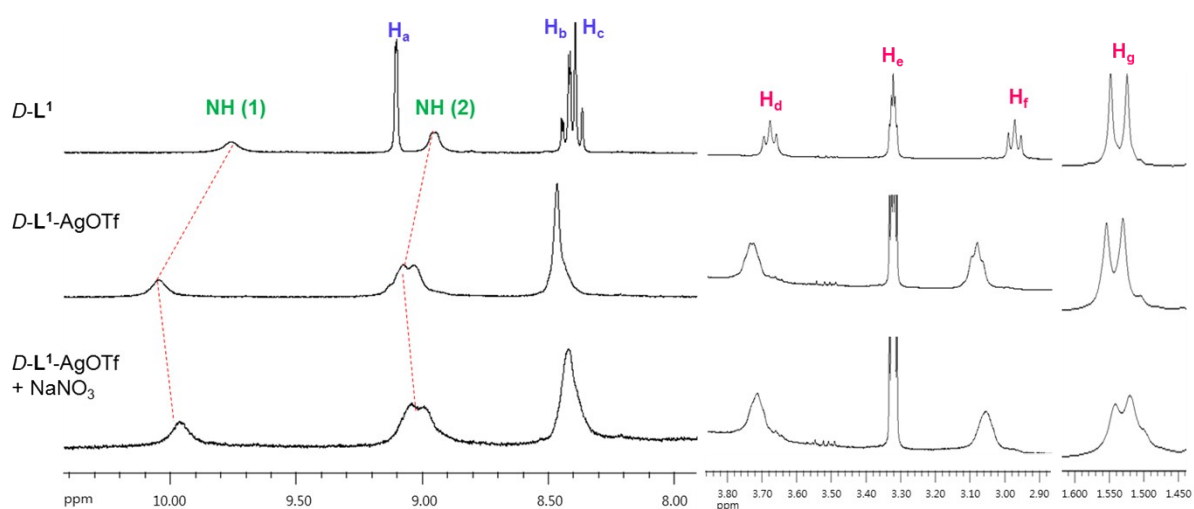


**Fig. S26** <sup>1</sup>H-NMR spectra obtained by addition of NaNO<sub>3</sub> (1.0 equiv.) in the presence of *D-L*<sup>1</sup> (8 mM) and AgOTf (1.0 equiv.) in MeOD and H<sub>2</sub>O (1:1 v/v).

**Additional Explanation;** The chemical shift of the amide protons (-NH) of *D-L*<sup>1</sup> were also observed upon addition of Ag<sup>+</sup> in a mixture of MeOD and H<sub>2</sub>O (1:1 v/v) due to the very slow hydrogen-deuterium exchange of NH protons. The amide (-NH) proton of *D-L*<sup>1</sup> was shifted to the low field ( $\Delta\delta = 0.29$  ppm) upon addition of AgOTf (1.0 equiv.). This unusually large shifting of the amide protons of *D-L*<sup>1</sup> with AgOTf (1.0 equiv.) in MeOD and H<sub>2</sub>O (1:1 v/v) was due to the formation of a favorable preorganized structure that enables the formation of intermolecular hydrogen bonds between the amide groups of *D-L*<sup>1</sup>. The amide (-NH) protons were returned to the high field upon addition of NaNO<sub>3</sub>, implying that the intermolecular hydrogen-bonding interactions between *D-L*<sup>1</sup> and *D-L*<sup>1</sup> were weakened due to the linkage with NO<sub>3</sub><sup>-</sup> between the hydrazine moiety of *D-L*<sup>1</sup> and *D-L*<sup>1</sup>. In contrast, the hydrazine (-NH) and alcoholic protons were not observed due to their overlapping with the H<sub>2</sub>O peak.

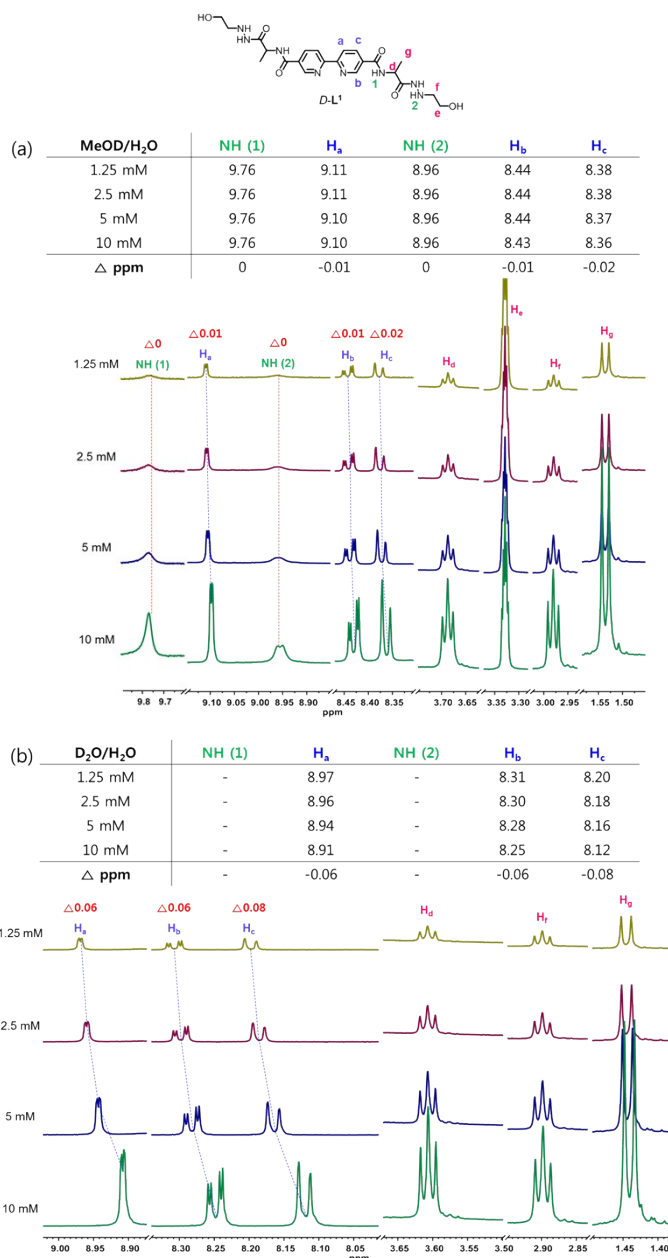


**Fig. S27** Concentration-dependent <sup>1</sup>H-NMR spectra of pristine *D-L*<sup>1</sup> (8 mM) in (a) MeOD and H<sub>2</sub>O (1:1 v/v) (b) D<sub>2</sub>O and H<sub>2</sub>O (1:1 v/v).

**Additional Explanation;** No chemical shift of the –NH protons in *D-L*<sup>1</sup> was observed. While, the aromatic protons were shifted to high field ( $\Delta\delta = -0.06$  ppm) due to the formation of  $\pi$ – $\pi$  stacking. The findings imply that the self-assembly of pristine *D-L*<sup>1</sup> occurred by  $\pi$ – $\pi$  stacking.

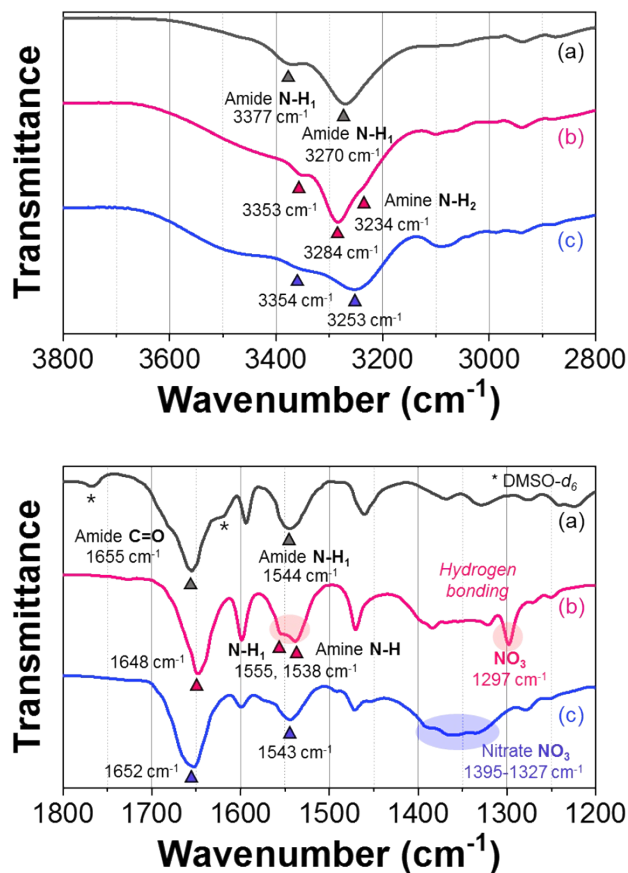


**Fig. S28** IR spectrum of (a) *D-L*<sup>1</sup> (black line), (b) the aggregate II (red line), and (c) the aggregate I (blue line). The NO<sub>3</sub><sup>-</sup> anion formed the intermolecular hydrogen-bonds with amine proton of hydrazine groups attached in *D-L*<sup>1</sup>.

**Additional Explanation;** The amide I (-C=O) band of aggregate II was shifted to low wavenumber, which was attributed to intermolecular hydrogen-bonding interactions between the amide groups of *D-L*<sup>1</sup>. Interestingly, one amide II band of *D-L*<sup>1</sup> appeared at 1544 cm<sup>-1</sup> was split into two bands at 1555 cm<sup>-1</sup> and 1538 cm<sup>-1</sup> in aggregate II, which correspond to the amide NH and hydrazine NH, respectively. The frequency changes of the N-H stretching bands of aggregate II at around 3284 cm<sup>-1</sup> showed also the same tendency as the amide II band at around 1555 cm<sup>-1</sup>. The low frequency shift of the hydrazine-NH band occurred due to linkage formation with the intermolecular hydrogen bonds between the hydrazine NH and the NO<sub>3</sub><sup>-</sup> in the chiral supramolecular polymers (aggregate II). However, the amide I (-C=O) band of aggregate I was no significantly shifted compared with that for *D-L*<sup>1</sup>. The hydrazine-N-H band (*ca.* 1543 cm<sup>-1</sup>) of aggregate I appeared at high wavenumber compared to that of aggregate II, indicating that the intermolecular hydrogen bonds within aggregate I is weaker than that of aggregate II. In particular, the broad AgNO<sub>3</sub> band at 1395–1327 cm<sup>-1</sup> showed a characteristic *D*<sub>3h</sub> symmetry,<sup>[13]</sup> whereas the sharp NO<sub>3</sub><sup>-</sup> band of aggregate II at 1297 cm<sup>-1</sup> showed *C*<sub>2v</sub> symmetry,<sup>[13]</sup> which also provides evidence for the intermolecular hydrogen binding of NO<sub>3</sub><sup>-</sup> in *D-L*<sup>1</sup>.

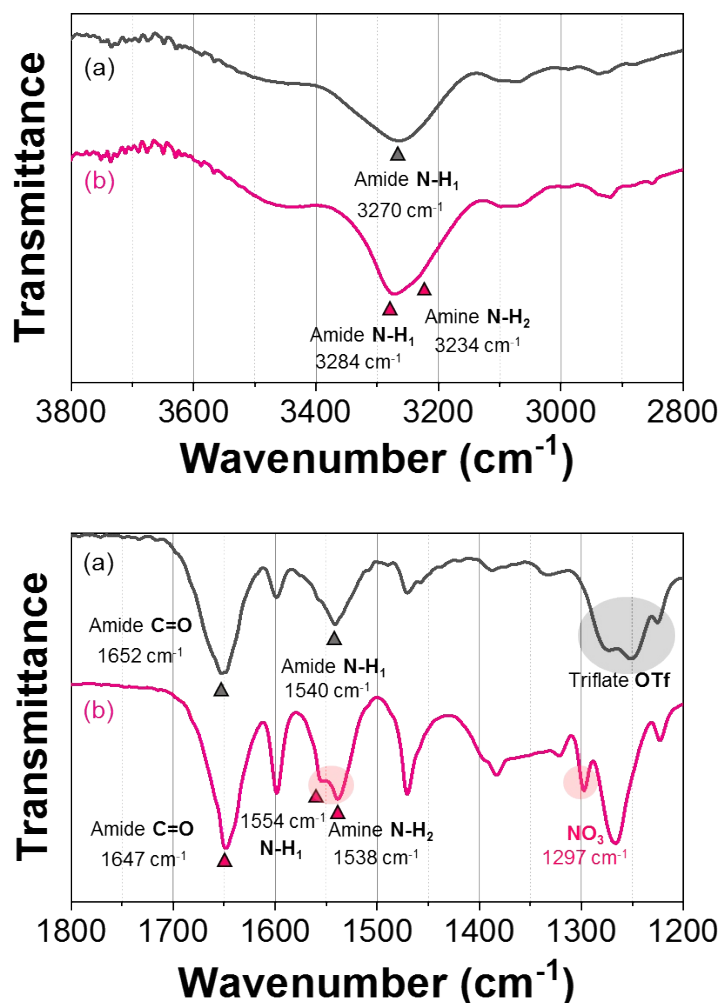


**Fig. S29** IR spectra of (a) the  $(D-L^1)_3Ag_2^{2+}$  complex formed by AgOTf and (b) the aggregate II formed by  $NaNO_3$  in the presence of the the  $(D-L^1)_3Ag_2^{2+}$  complex formed by AgOTf.

**Additional Explanation;** The amide I band of aggregate II ( $(D-L^1)_3Ag_2(NO_3)_2$  complex) that formed via addition of  $NaNO_3$  to  $D-L^1$  in the presence of AgOTf (1.0 equiv.) shifted from  $1652\text{ cm}^{-1}$  to  $1647\text{ cm}^{-1}$ , whereas the single amide II band of  $D-L^1$  with AgOTf at  $1540\text{ cm}^{-1}$  was separated into two bands at  $1554\text{ cm}^{-1}$  and  $1538\text{ cm}^{-1}$ , which correspond to the amide NH and the hydrazine NH, respectively. A relatively large frequency change for the hydrazine–NH stretching band of  $D-L^1$  was also observed upon addition of  $NaNO_3$  in the presence of AgOTf (1.0 equiv.). Notably, aggregate II was formed by the interaction between the hydrazine NH of  $D-L^1$ , the  $NO_3^-$  anion, and the–NH of  $D-L^1$ .

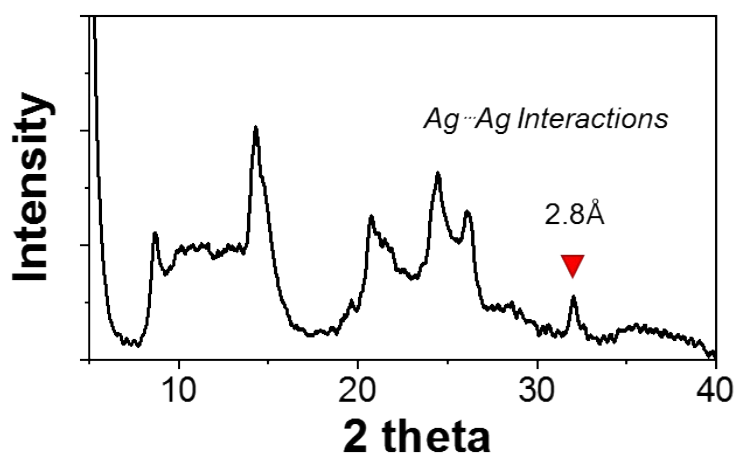


**Fig. S30** Powder XRD pattern of the aggregate II based on the  $(D-L^1)_3Ag_2(NO_3)_2$  in water.

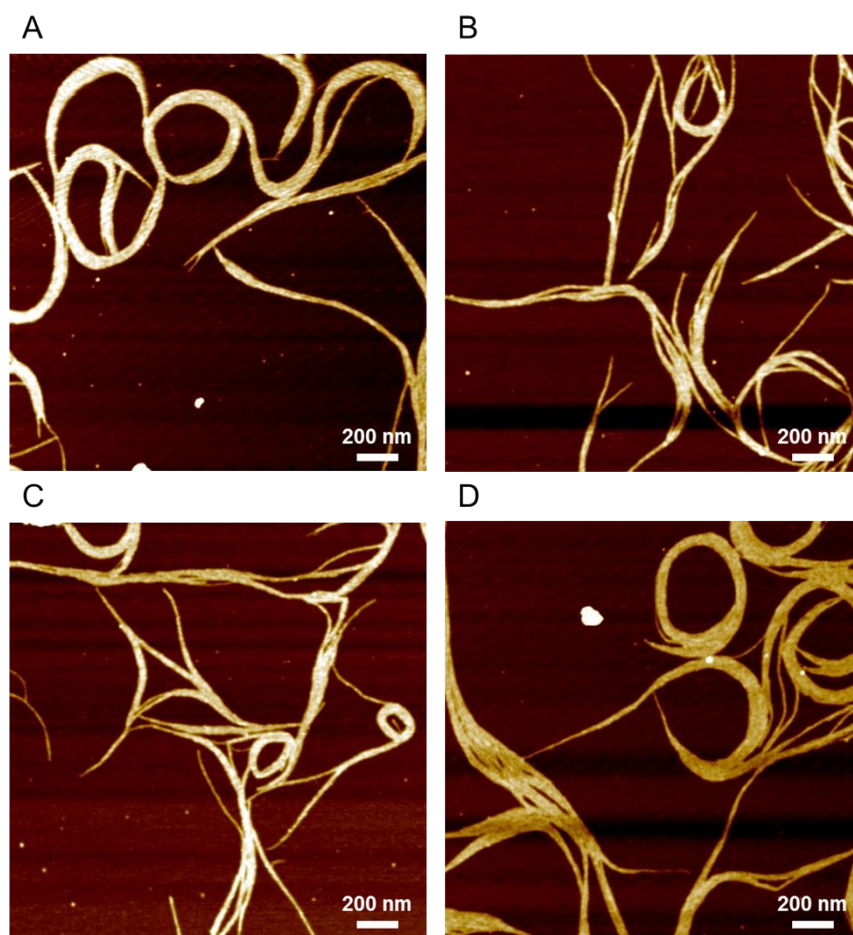


**Fig. S31** Time-dependent AFM images of pristine  $D-L^1$  (8 mM) in water after aging for (A) 10 min., (B) 90 min., (C) 120 min., and (D) 2 weeks.

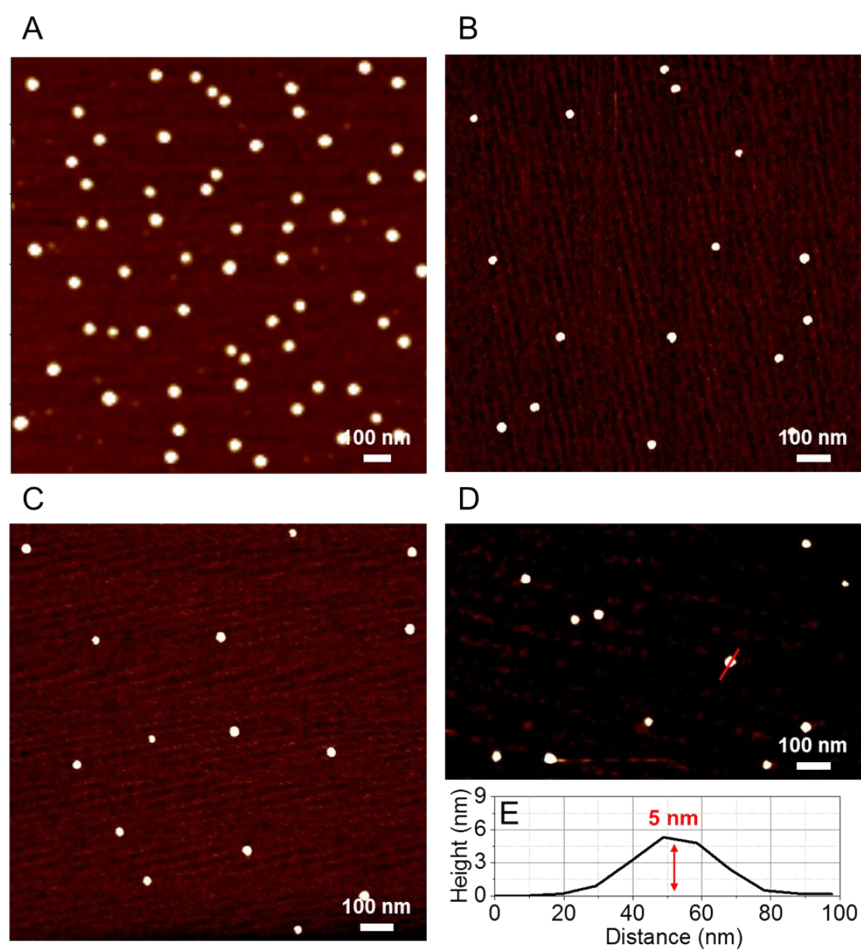


**Fig. S32** Time-dependent AFM images of the aggregate I produced in a mixture of *D-L*<sup>1</sup> (8 mM) and AgNO<sub>3</sub> (2.0 equiv.) in water after aging for (A) 10 min., (B) 90 min., (C) 120 min., and (D) 2 weeks. (E) Height of nanoparticles measured by AFM.

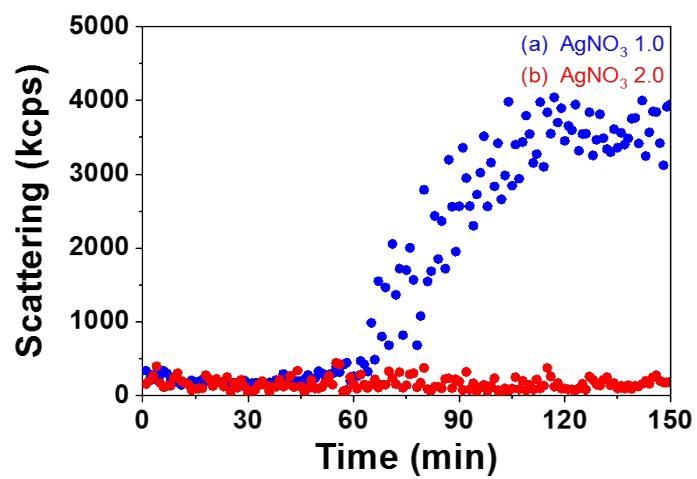


**Fig. S33** Time-dependent DLS measurements of *D-L*<sup>1</sup> (8 mM) in the presence of AgNO<sub>3</sub> (a) 1.0 equiv.(blue line) and (b) 2.0 equiv.(red line) in water.

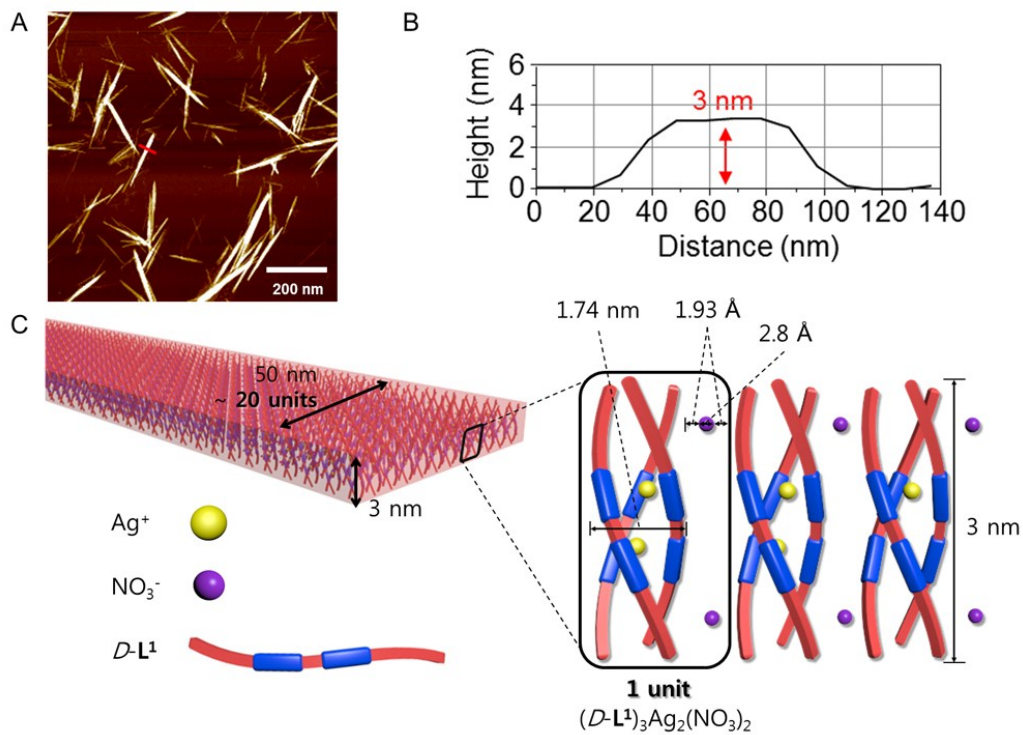


**Fig. S34** (A) AFM image and (B) the thickness of the aggregate II obtained by *D-L*<sup>1</sup> (8 mM) and AgNO<sub>3</sub> (0.5-1.3 equiv.) after aging for 120 min. (C) Proposed structure for molecular arrangement of the aggregate II based on AFM and DFT calculation.

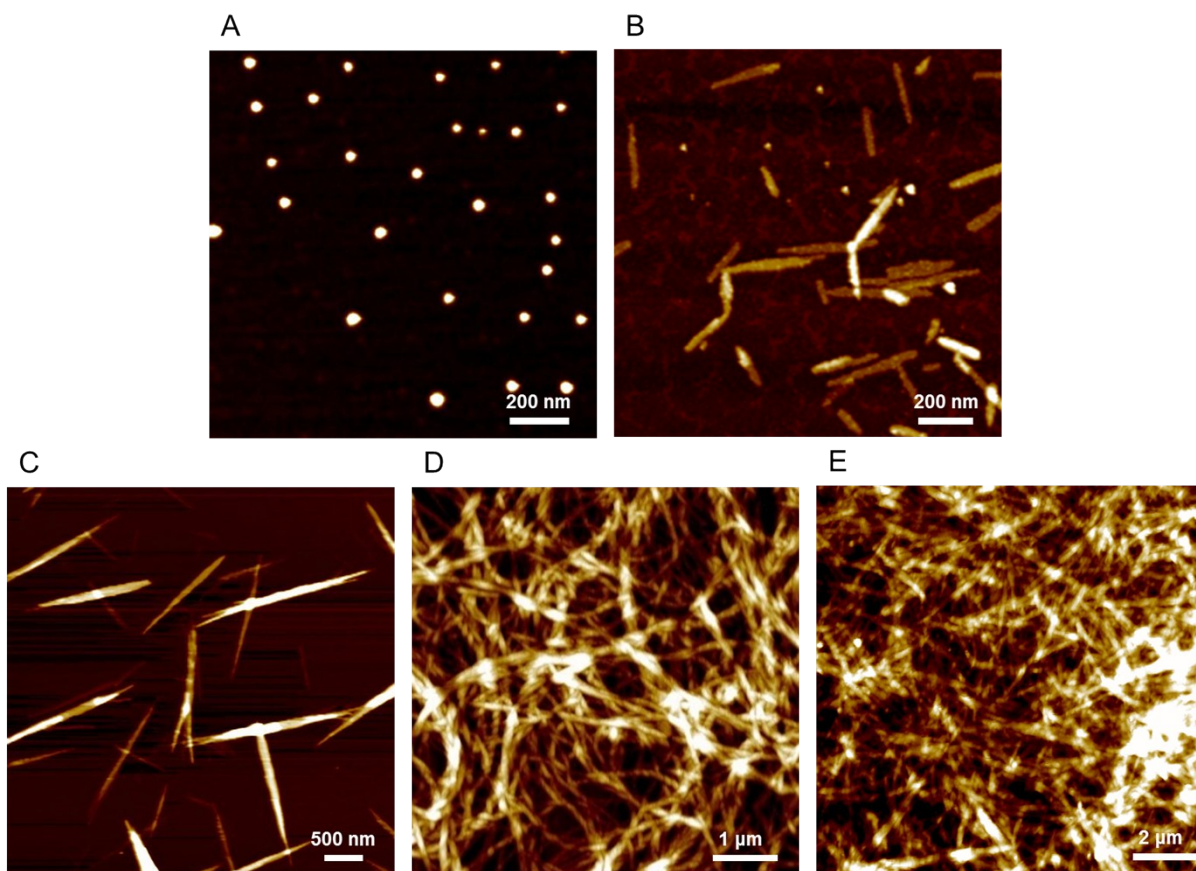


**Fig. S35** Time-dependent AFM images of *D-L*<sup>1</sup> (8 mM) with AgNO<sub>3</sub> (1.3 equiv.) by aging for (A) 10 min., (B) 90 min., (C) 120 min., (D) 180 min., and (E) 2 weeks.

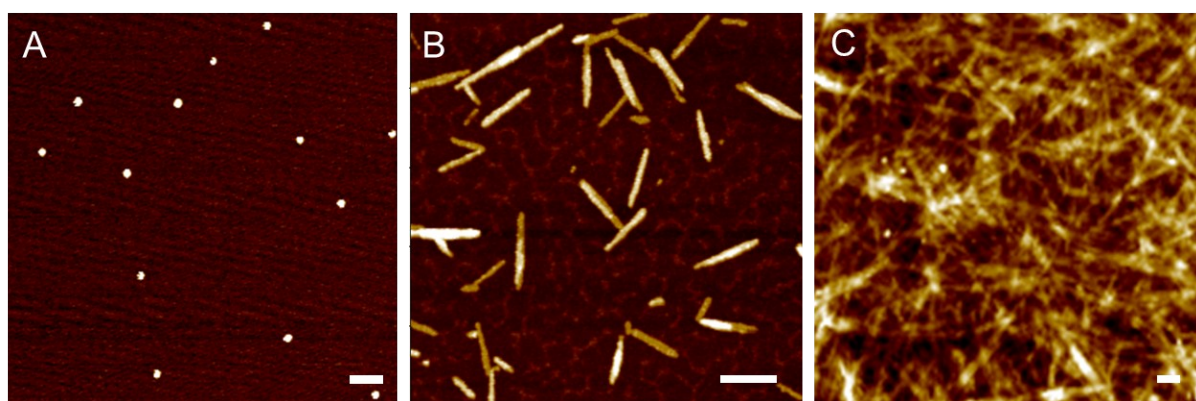


**Fig. S36** AFM images of *D-L*<sup>1</sup> (8 mM) with 2.0 equiv. of NaNO<sub>3</sub> in the presence of 1.0 equiv. of AgOTf in water after aging for (A) 0, (B) 30 min., and (C) 60 min. Scale bars, 200 nm.

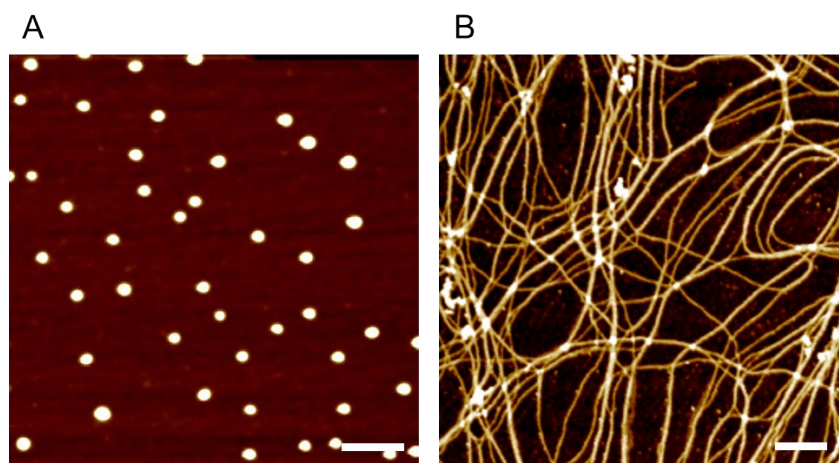


**Fig. S37** AFM images of (A) the aggregate I based on the  $D\text{-L}^2\text{AgNO}_3$  complex, and (B) the aggregate II based on the  $(D\text{-L}^2)_3\text{Ag}_2(\text{NO}_3)_2$  complex. Scale bars, 200 nm.

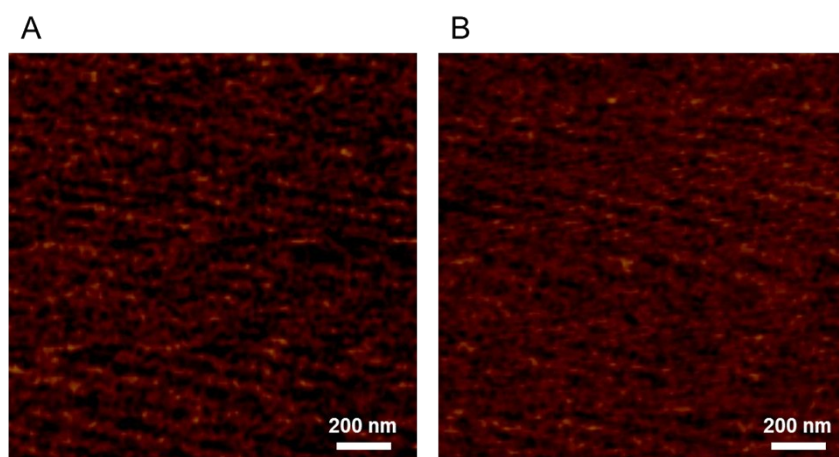


**Fig. S38** AFM images of  $D\text{-L}^3$  (8 mM) (A) without and (B) with 1.0 equiv. of  $\text{AgNO}_3$ .

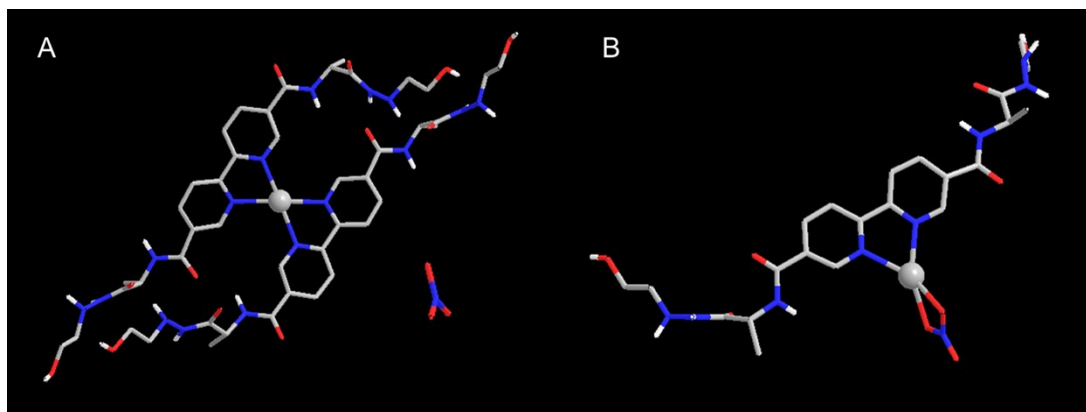


**Fig. S39** Optimized structures of (A)  $(D-L^1)_2AgNO_3$  (B)  $D-L^1AgNO_3$ . The  $NO_3^-$  anion was not coordinated to  $Ag^+$  ion in the  $(D-L^1)_2AgNO_3$  complex.

**Additional Explanation;** We also obtained the complex formation energies for the three complexes calculated assuming the following simple process:  $m(D-L^1) + nAg^+ + k(NO_3^-) \rightarrow (D-L^1)_mAg_n(NO_3^-)_k$ . The complex formation energy ( $\Delta E_{cf}$ ) is obtained by  $\Delta E_{cf} = (m \times E(D-L^1)) + (n \times E(Ag^+)) + (k \times E(NO_3^-)) - E[(D-L^1)_mAg_n(NO_3^-)_k]$ , where  $E(X)$  is the calculated energy of  $X$  ( $X = D-L^1, Ag^+, NO_3^-$ , and complexes  $[(D-L^1)_mAg_n(NO_3^-)_k]$ ). The  $\Delta E_{cf}$  values for  $D-L^1AgNO_3$ ,  $(D-L^1)_2AgNO_3$ , and  $(D-L^1)_3Ag_2(NO_3)_2$  are calculated to be 51.8, 62.1, and 118.0 kcal/mol, respectively. Thus, the  $(D-L^1)_3Ag_2(NO_3)_2$  complex was the most stable. There are two hydrogen bonds between the ligands and two  $NO_3^-$  moieties in the 3:2  $(D-L^1:Ag^+)$  complex. Thus, the average binding energy of the hydrogen bond is *ca.* 8 kcal/mol, which is a typical bond strength for intermolecular hydrogen bonds.<sup>[14]</sup> In addition, the calculated structure of  $(D-L^1)_3Ag_2(NO_3)_2$  demonstrated right-handed helicity, which supports the fact that the right-handed complex is the thermodynamic product and the helicity inversion from left- to right-handed occurred upon aging, as observed experimentally. We also proposed a structure unit of the supramolecular polymer (aggregate II) based on the  $(D-L^1)_3Ag_2(NO_3)_2$  complex with right-handed helicity shown in Fig. 6B, which is constructed using four building block units. The helicity of the proposed structure is consistent with the CD observations.

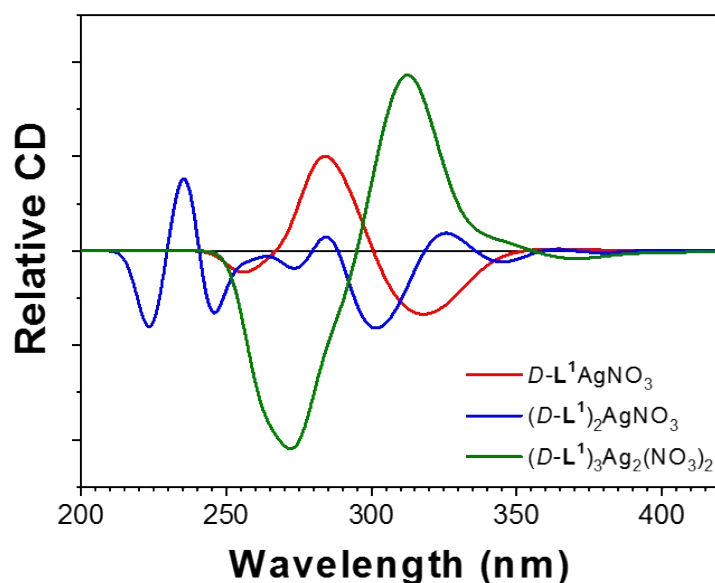


**Fig. S40** Calculated CD spectra of  $D\text{-L}^1\text{AgNO}_3$ ,  $(D\text{-L}^1)_2\text{AgNO}_3$ , and  $(D\text{-L}^1)_3\text{Ag}_2(\text{NO}_3)_2$ . The  $\text{NO}_3^-$  anion was not coordinated to  $\text{Ag}^+$  ion in the  $(D\text{-L}^1)_2\text{AgNO}_3$  complex.

**Additional Explanation;** To understand the inversion of the CD spectra obtained experimentally with different  $\text{AgNO}_3$  concentrations, we calculated simulated CD spectra for the  $D\text{-L}^1\text{AgNO}_3$ ,  $(D\text{-L}^1)_2\text{Ag}^+$ , and  $(D\text{-L}^1)_3\text{Ag}_2(\text{NO}_3)_2$  complexes. The CD spectra were calculated using time-dependent DFT (TDDFT)<sup>[2,3]</sup> considering excitation up to 200 singlet excited states. Negative CD signals were obtained at *ca.* 302 nm for the  $(D\text{-L}^1)_2\text{AgNO}_3$  complex and at *ca.* 318 nm for the  $D\text{-L}^1\text{AgNO}_3$  complex. In contrast, the  $(D\text{-L}^1)_3\text{Ag}_2(\text{NO}_3)_2$  complex demonstrated an intense positive CD signal at *ca.* 312 nm. Therefore, the calculated CD spectra are consistent with the experimental results, i.e., CD inversion originates from formation of the  $(D\text{-L}^1)_3\text{Ag}_2(\text{NO}_3)_2$  complex.

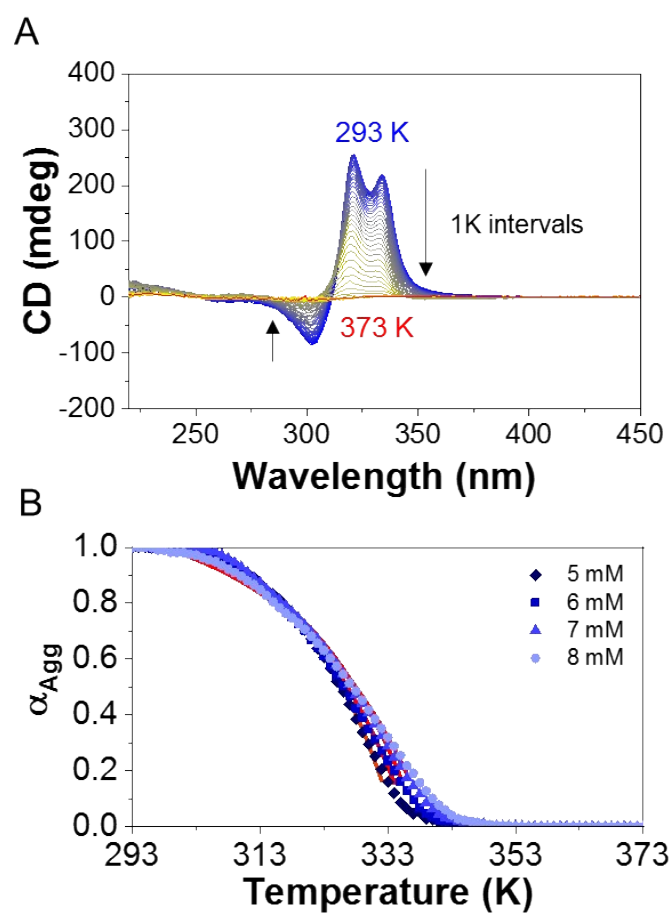


**Fig. S41** (A) Temperature-dependent CD spectra of *D-L*<sup>1</sup> (8 mM) with 1.0 equiv. of AgNO<sub>3</sub> by heating in water. (B) Degree of aggregation of different concentrations of *D-L*<sup>1</sup> (5-8 mM) complex with 1.0 equiv. of AgNO<sub>3</sub> as a function of temperature at 334 nm in water.

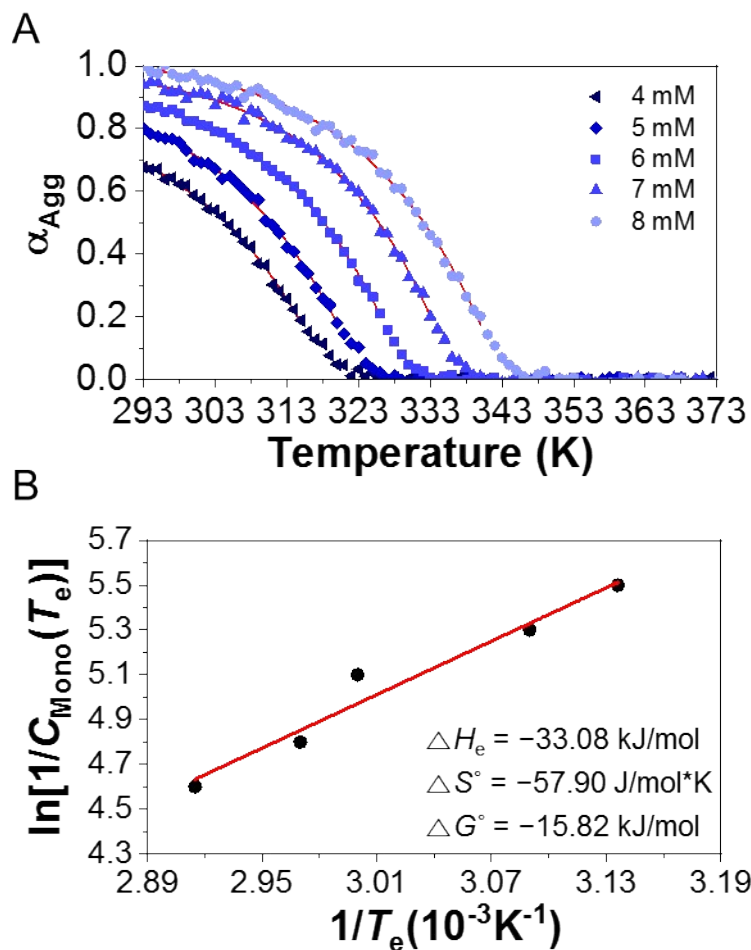


**Fig. S42** (A) Degree of aggregation of different concentrations of *D-L*<sup>1</sup> complex with 2.0 equiv. of AgNO<sub>3</sub> as a function of temperature at 334 nm in water. (B) Natural logarithm of the reciprocal  $C_T$  as a function of the reciprocal  $T_e$  showing the linear relationship.

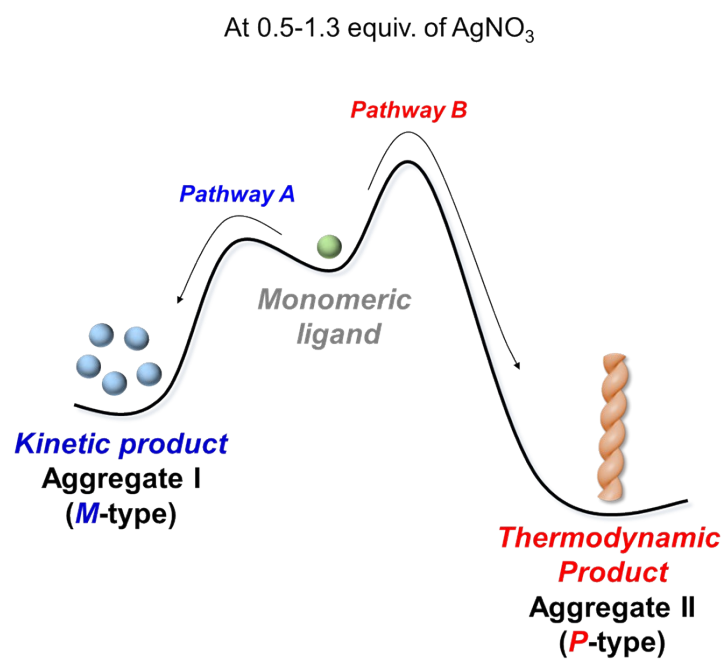


**Fig. S43** Energy landscape diagram of the aggregates I and II based on  $D\text{-L}^1$  in the presence of 0.5-1.3 equiv. of  $\text{AgNO}_3$  in water.

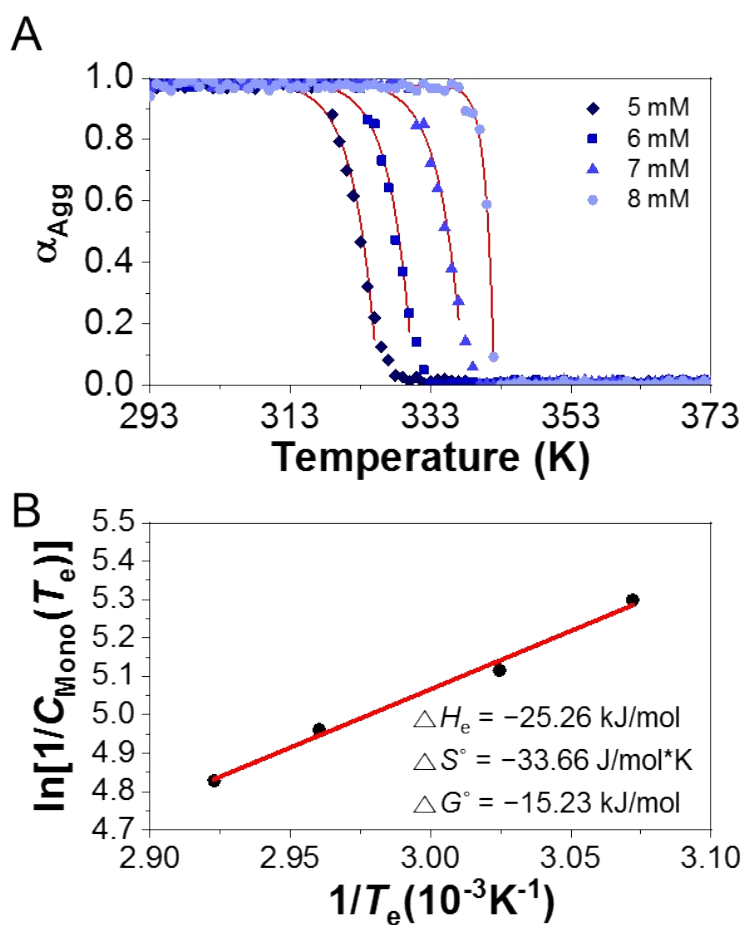


**Fig. S44** (A) Degree of aggregation of different concentrations of pristine *D-L*<sup>1</sup> as a function of temperature at 336.5 nm by cooling rate of 1 K min<sup>-1</sup> in water. (B) Natural logarithm of the reciprocal  $C_T$  as a function of the reciprocal  $T_e$  showing the linear relationship.

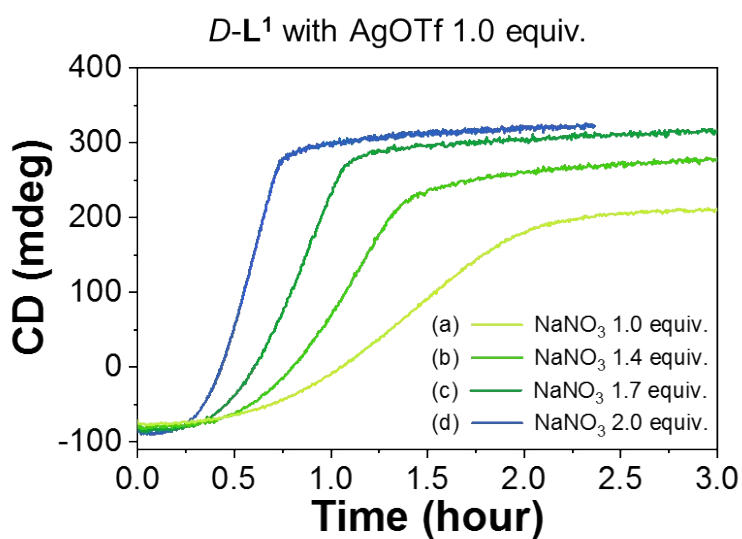


**Fig. S45** Kinetic profiles of the CD intensity of *D-L*<sup>1</sup> (8 mM) with (a) 1.0 (b) 1.4 (c) 1.7 and (d) 2.0 equiv. of NaNO<sub>3</sub> in the presence of AgOTf (1.0 equiv.) at 334 nm in water.

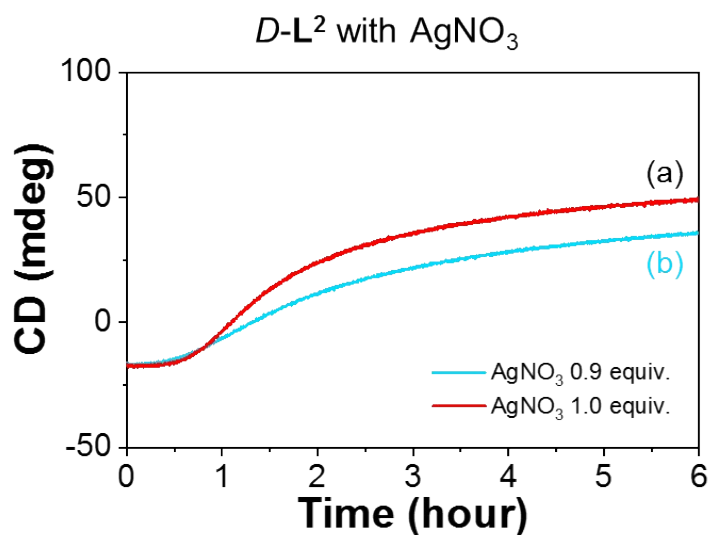


**Fig. S46** Kinetic profiles of the CD intensity of *D-L*<sup>2</sup> (8 mM) with (a) 0.9 and (b) 1.0 equiv. of AgNO<sub>3</sub> at 334 nm in water.

## 4. Analytic data

### 4.1 $^1\text{H}$ -NMR and $^{13}\text{C}$ -NMR spectroscopy

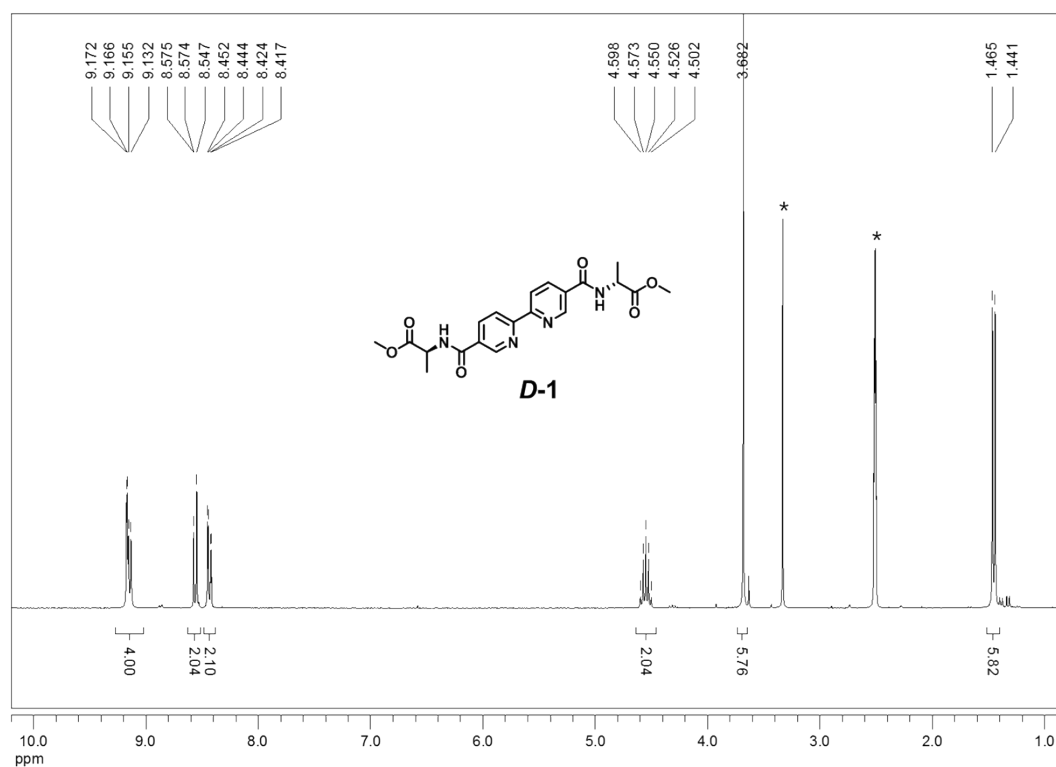


**Fig. S47**  $^1\text{H}$  NMR spectrum (300 MHz) of **D-1** in  $\text{DMSO-}d_6$  at 25 °C.

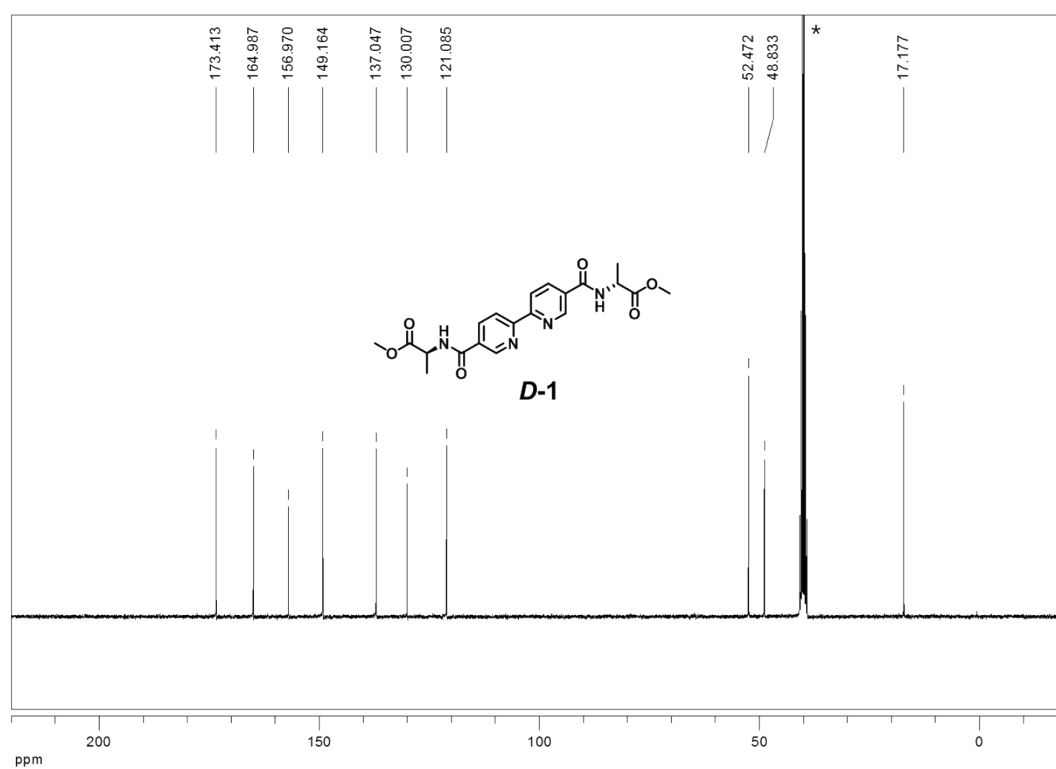


**Fig. S48**  $^{13}\text{C}$  NMR spectrum (75 MHz) of **D-1** in  $\text{DMSO-}d_6$  at 25 °C.

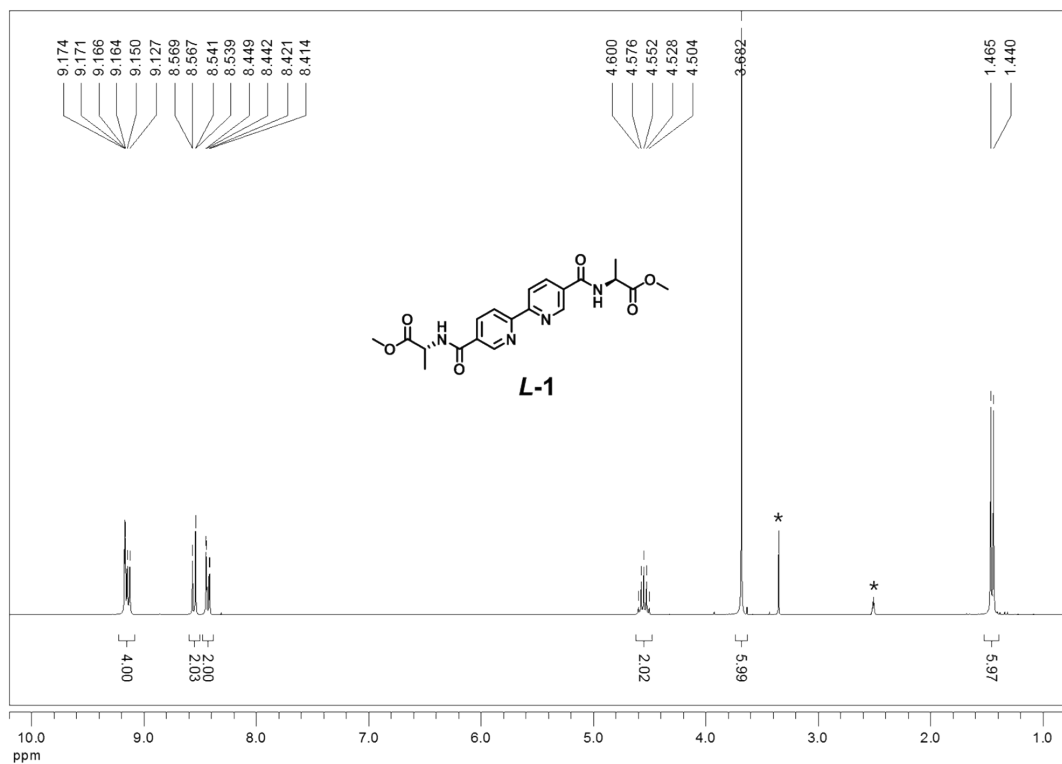


**Fig. S49**  $^1\text{H}$  NMR spectrum (300 MHz) of **L-1** in  $\text{DMSO-}d_6$  at 25 °C.

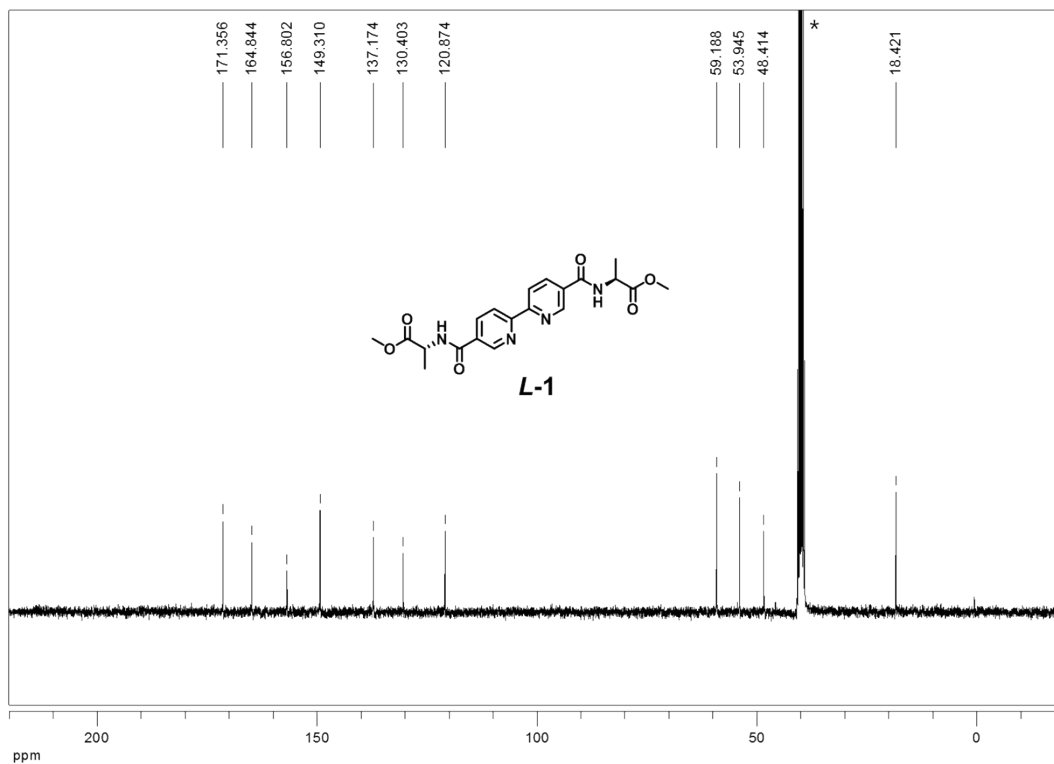


**Fig. S50**  $^{13}\text{C}$  NMR spectrum (75 MHz) of **L-1** in  $\text{DMSO-}d_6$  at 25 °C.

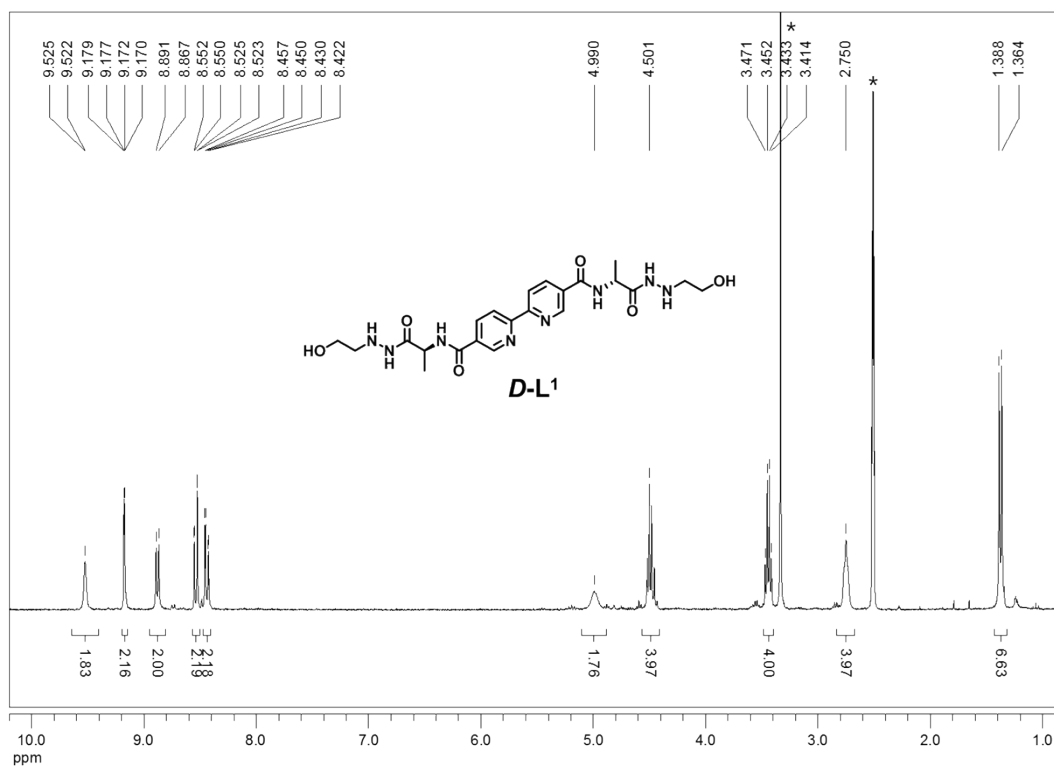


**Fig. S51** <sup>1</sup>H NMR spectrum (300 MHz) of *D-L*<sup>1</sup> in DMSO-*d*<sub>6</sub> at 25 °C.

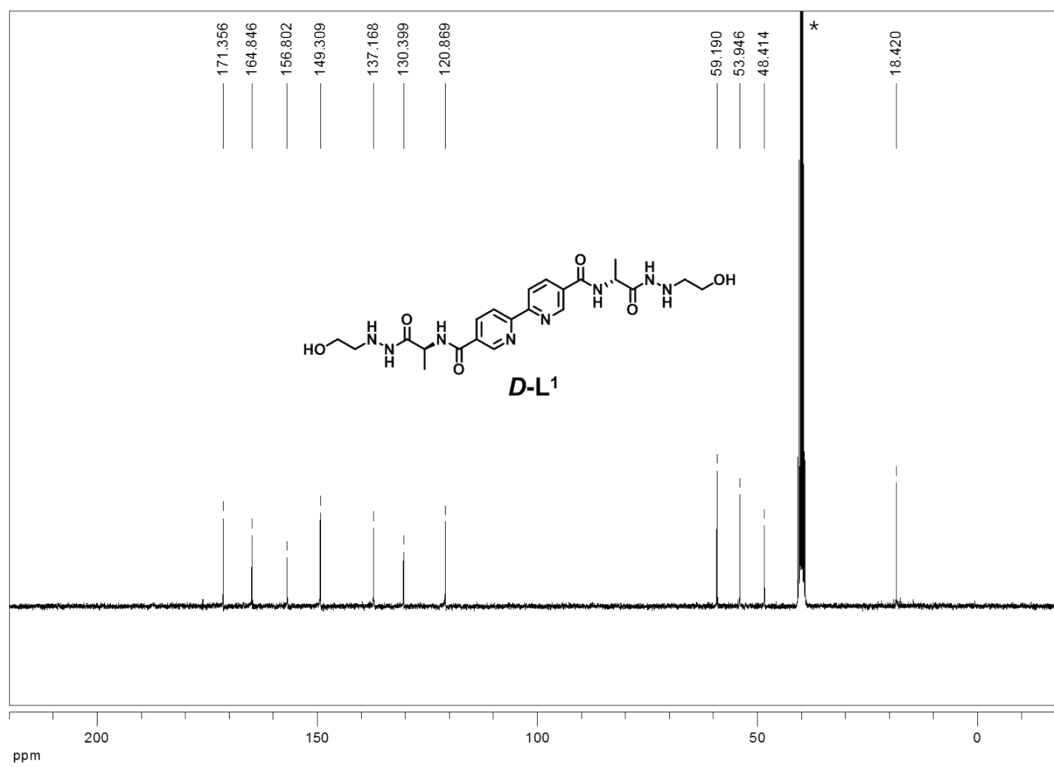


**Fig. S52** <sup>13</sup>C NMR spectrum (75 MHz) of *D-L*<sup>1</sup> in DMSO-*d*<sub>6</sub> at 25 °C.

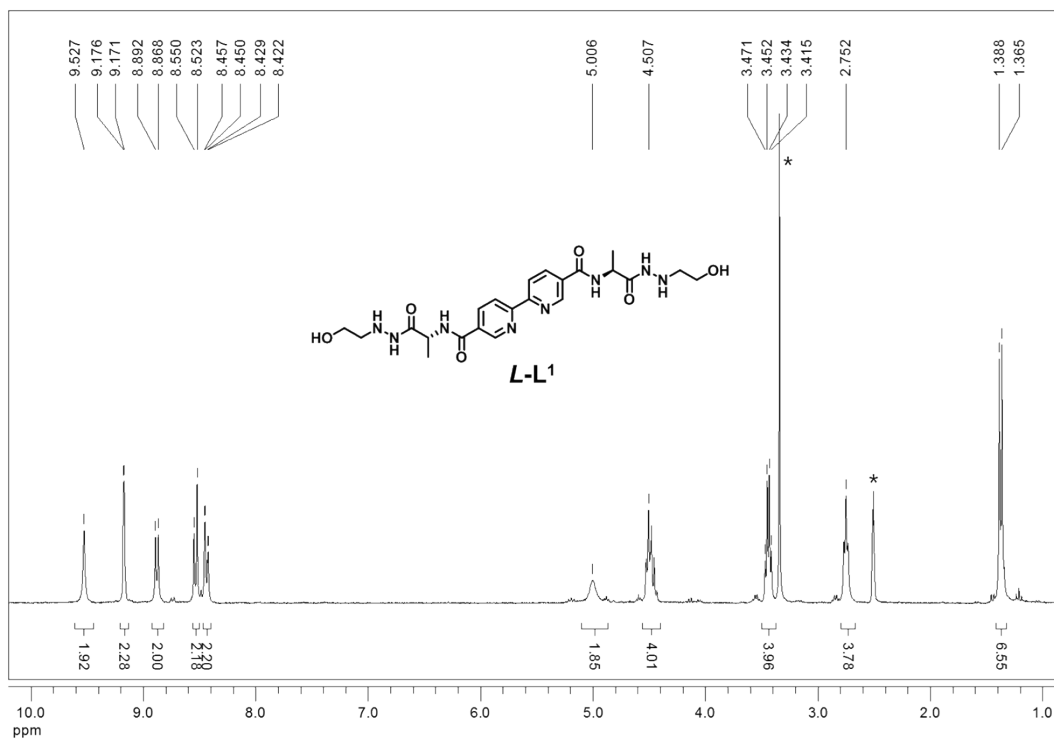


**Fig. S53** <sup>1</sup>H NMR spectrum (300 MHz) of *L-L*<sup>1</sup> in DMSO-*d*<sub>6</sub> at 25 °C.

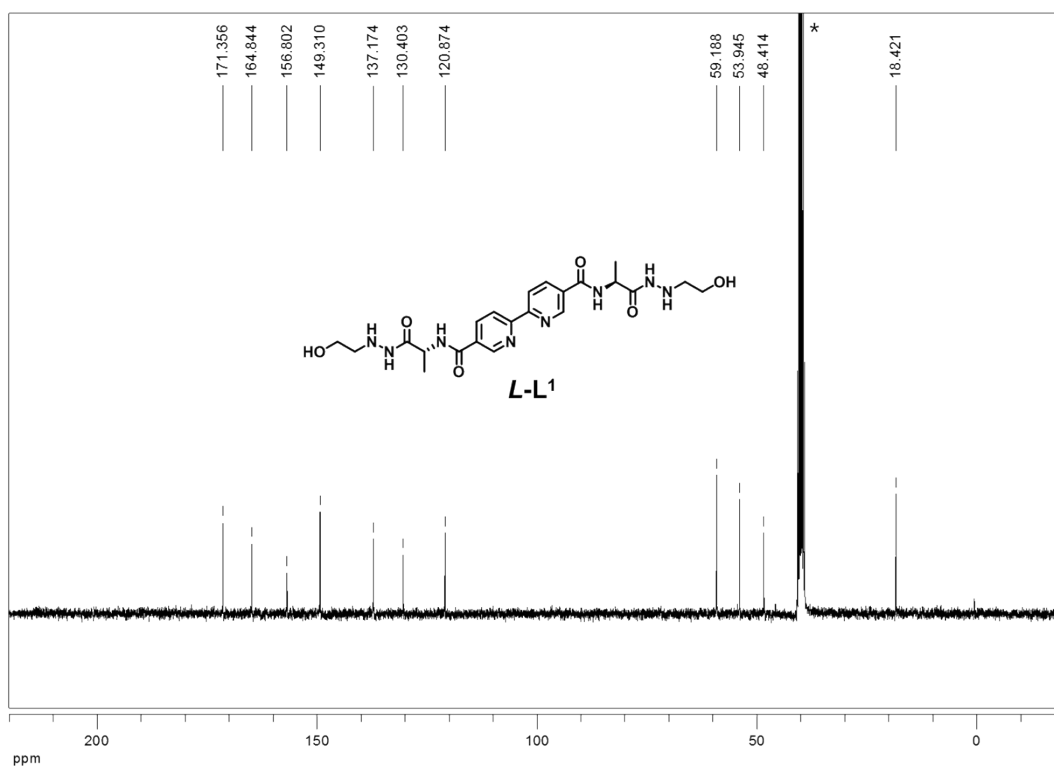


**Fig. S54** <sup>13</sup>C NMR spectrum (75 MHz) of *L-L*<sup>1</sup> in DMSO-*d*<sub>6</sub> at 25 °C.

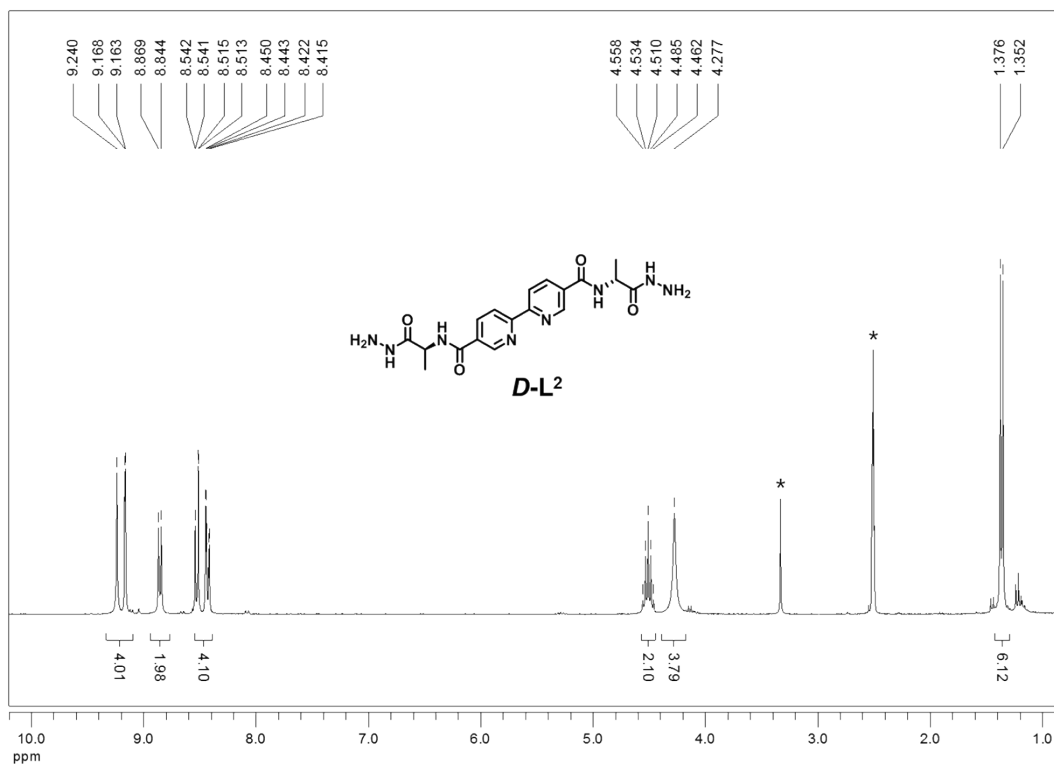


**Fig. S55** <sup>1</sup>H NMR spectrum (300 MHz) of **D-L<sup>2</sup>** in DMSO-*d*<sub>6</sub> at 25 °C.

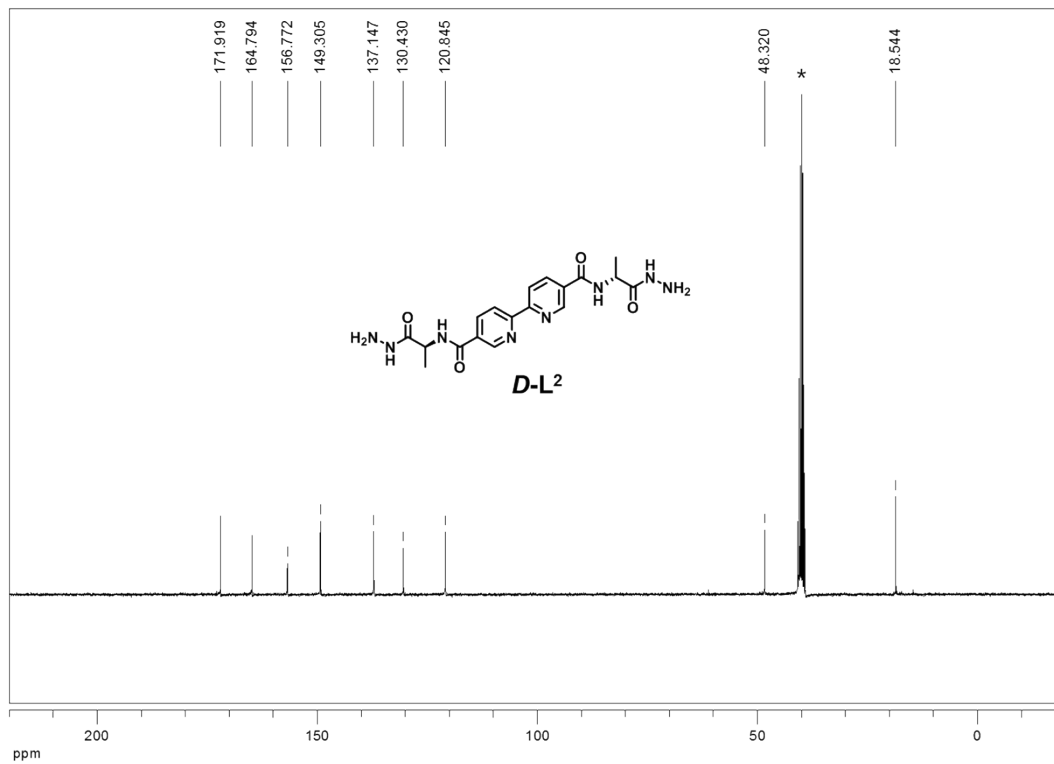


**Fig. S56** <sup>13</sup>C NMR spectrum (75 MHz) of **D-L<sup>2</sup>** in DMSO-*d*<sub>6</sub> at 25 °C.

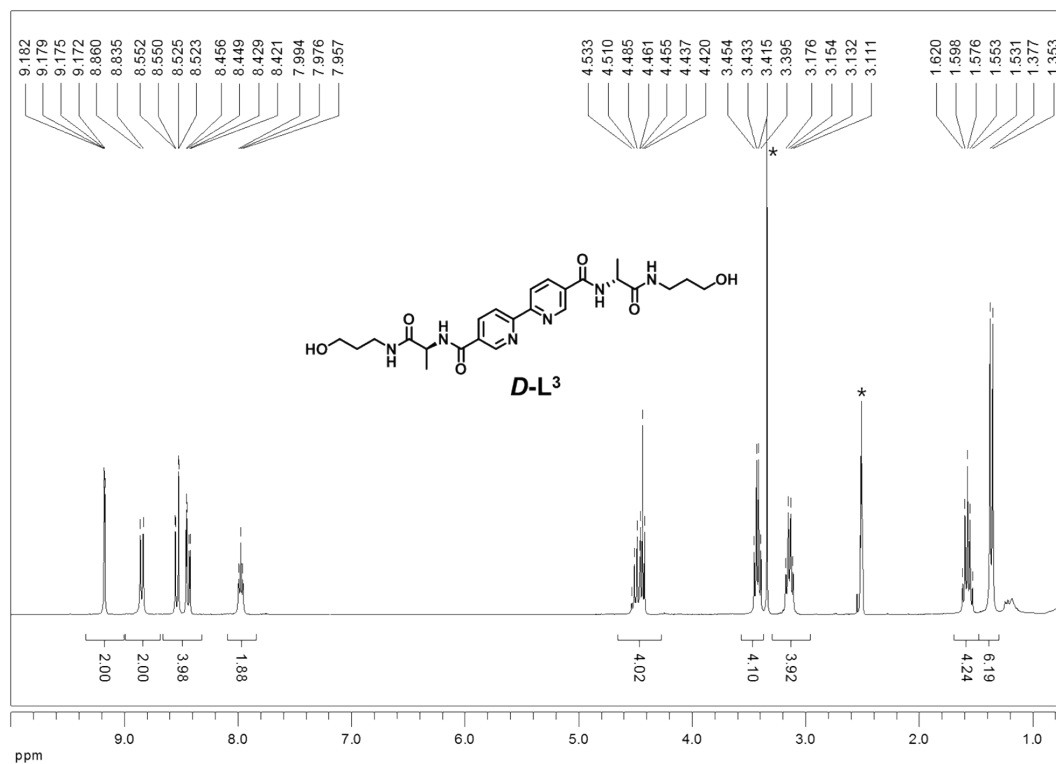


**Fig. S57** <sup>1</sup>H NMR spectrum (300 MHz) of *D-L*<sup>3</sup> in DMSO-*d*<sub>6</sub> at 25 °C.

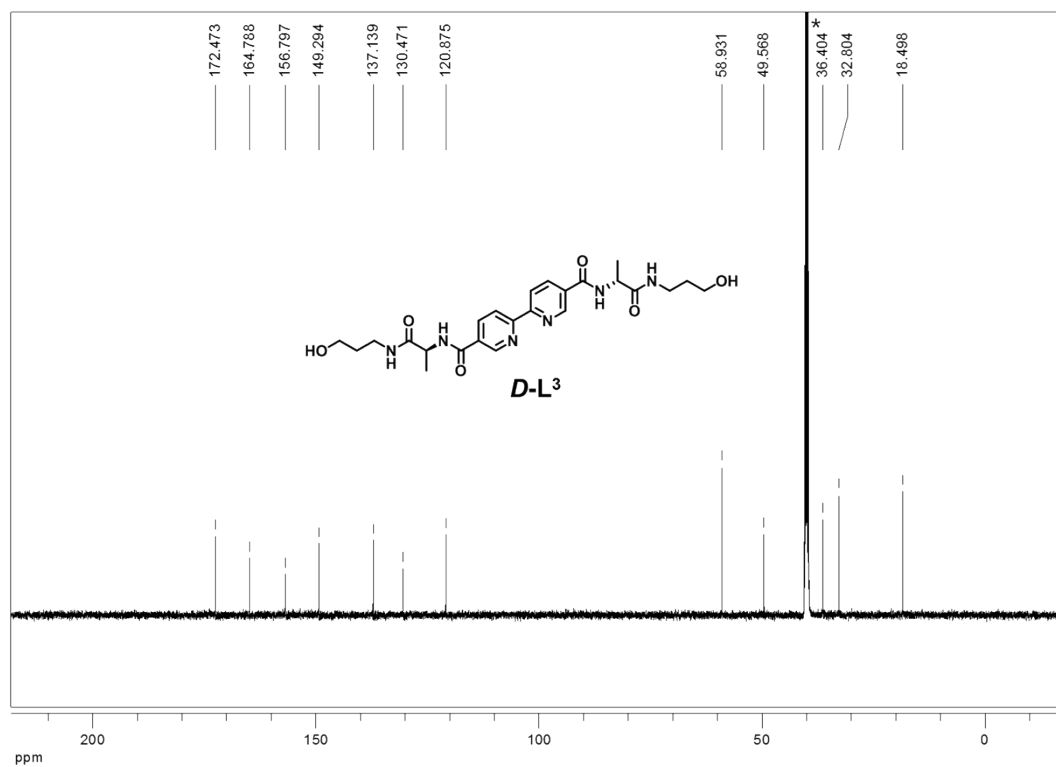


**Fig. S58** <sup>13</sup>C NMR spectrum (75 MHz) of *D-L*<sup>3</sup> in DMSO-*d*<sub>6</sub> at 25 °C.

## 4.2 HR ESI-MS spectrometry

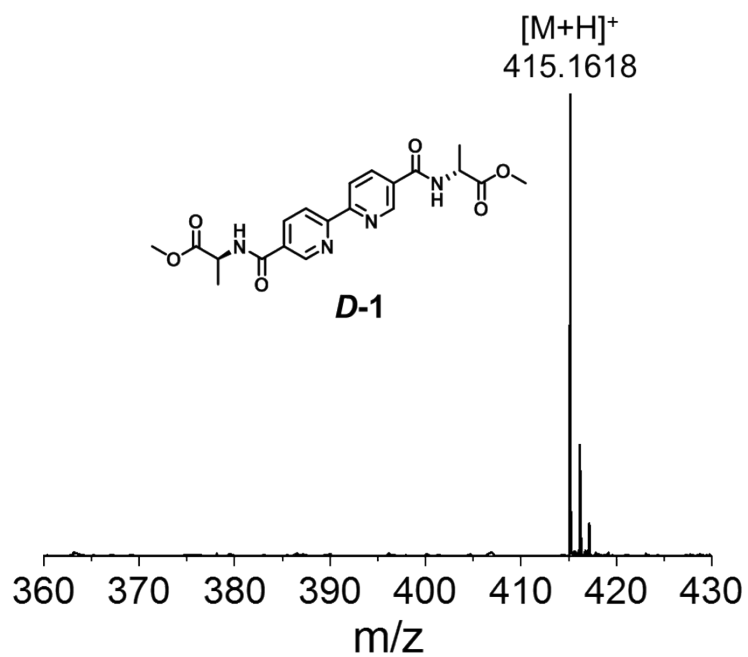


**Fig. S59** HR ESI-MS spectrum of **D-1** in water.

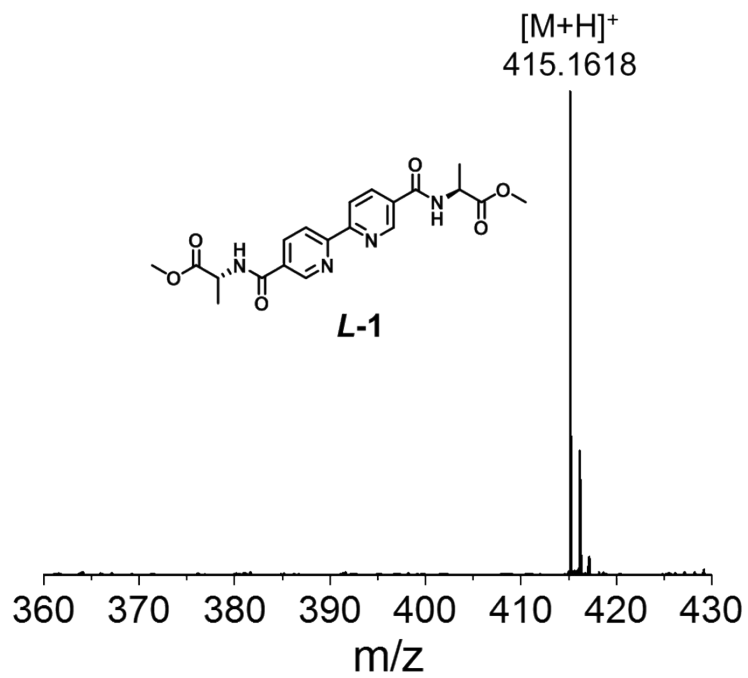


**Fig. S60** HR ESI-MS spectrum of **L-1** in water.

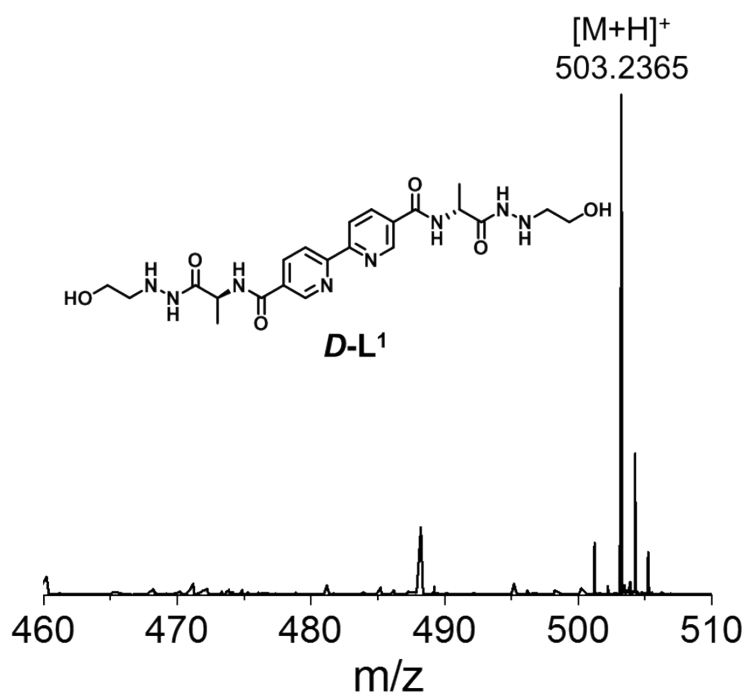


Fig. S61 HR ESI-MS spectrum of *D-L*<sup>1</sup> in water.

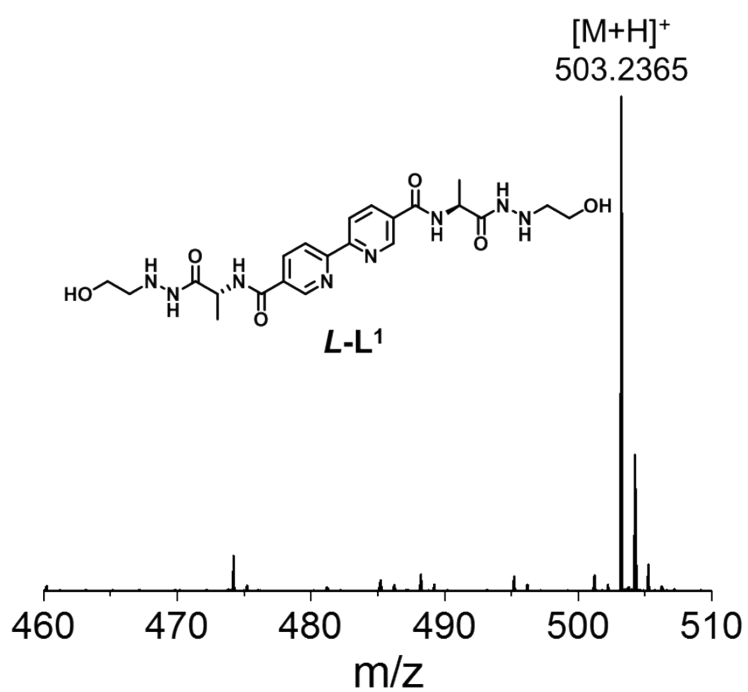
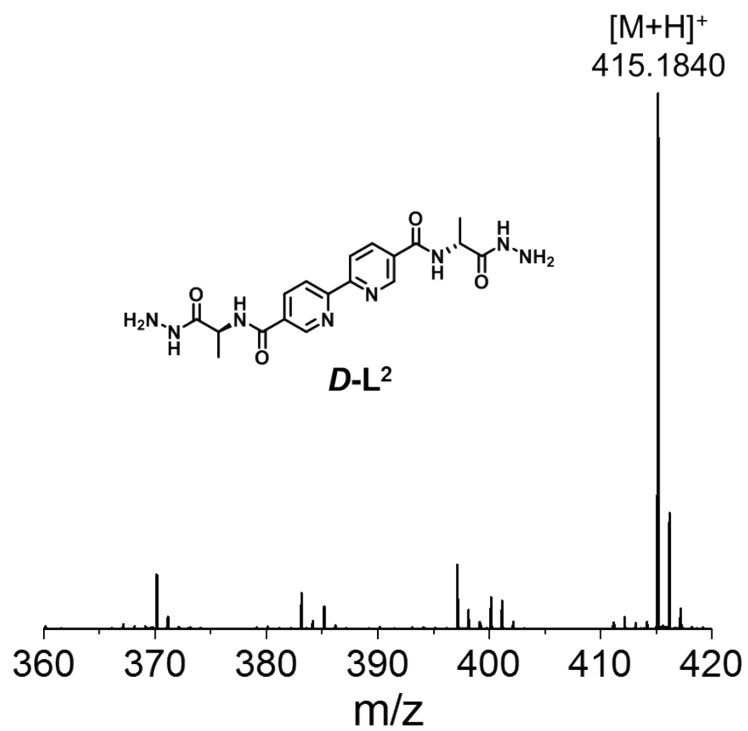
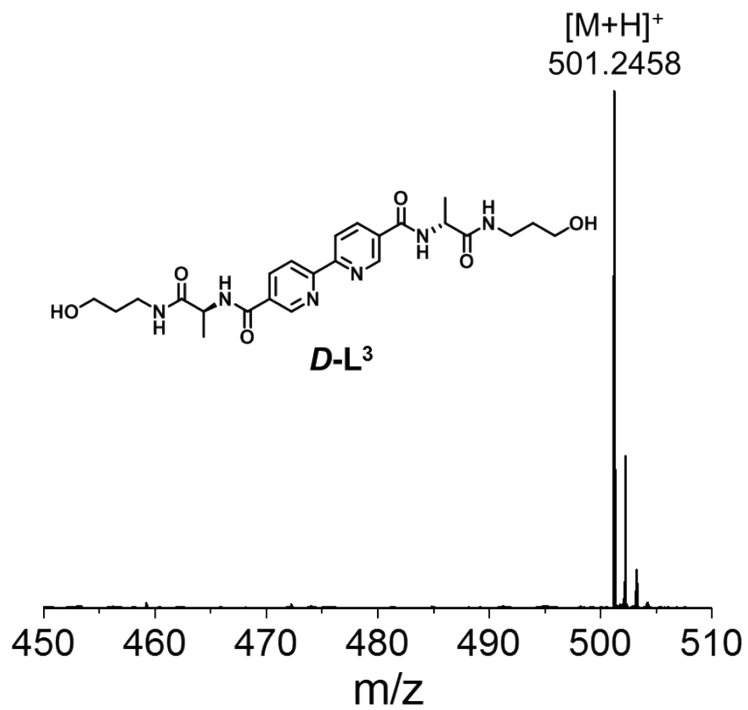


Fig. S62 HR ESI-MS spectrum of *L-L*<sup>1</sup> in water.



**Fig. S63** HR ESI-MS spectrum of **D-L<sup>2</sup>** in water.



**Fig. S64** HR ESI-MS spectrum of **D-L<sup>3</sup>** in water.

## 5. References

- [1] M. Wakabayashi, S. Yokojima, T. Fukaminato, K.-i. Shiino, M. Irie and S. Nakamura, *J. Phys. Chem. A*, 2014, **118**, 5046-5057.
- [2] E. Runge and E. K. U. Gross, *Phys. Rev. Lett.*, 1984, **52**, 997-1000.
- [3] A. D. Becke, *J. Chem. Phys.*, 1993, **98**, 5648-5652.
- [4] H. F. Schaefer, III and Editor, *Modern Theoretical Chemistry*, Vol. 3: Methods of Electronic Structure Theory, Plenum, 1977.
- [5] Frisch, M. J.; Trucks, G. W.; Schlegel, H. B.; Scuseria, G. E.; Robb, M. A.; Cheeseman, J. R.; Scalmani, G.; Barone, V.; Petersson, G. A.; Nakatsuji, H.; Li, X.; Caricato, M.; Marenich, A. V.; Bloino, J.; Janesko, B. G.; Gomperts, R.; Mennucci, B.; Hratchian, H. P.; Ortiz, J. V.; Izmaylov, A. F.; Sonnenberg, J. L.; Williams-Young, D.; Ding, F.; Lipparini, F.; Egidi, F.; Goings, J.; Peng, B.; Petrone, A.; Henderson, T.; Ranasinghe, D.; Zakrzewski, V. G.; Gao, J.; Rega, N.; Zheng, G.; Liang, W.; Hada, M.; Ehara, M.; Toyota, K.; Fukuda, R.; Hasegawa, J.; Ishida, M.; Nakajima, T.; Honda, Y.; Kitao, O.; Nakai, H.; Vreven, T.; Throssell, K.; Montgomery, J. A., Jr.; Peralta, J. E.; Ogliaro, F.; Bearpark, M. J.; Heyd, J. J.; Brothers, E. N.; Kudin, K. N.; Staroverov, V. N.; Keith, T. A.; Kobayashi, R.; Normand, J.; Raghavachari, K.; Rendell, A. P.; Burant, J. C.; Iyengar, S. S.; Tomasi, J.; Cossi, M.; Millam, J. M.; Klene, M.; Adamo, C.; Cammi, R.; Ochterski, J. W.; Martin, R. L.; Morokuma, K.; Farkas, O.; Foresman, J. B.; Fox, D. J. *Gaussian 16*, Revision B.01; Gaussian, Inc., Wallingford CT, **2016**.
- [6] D. D. Prabhu, K. Aratsu, H. Ouchi, S. Yagai, Y. Kitamoto, S. Yagai, T. Ohba, M. J. Hollamby, N. Shimizu, H. Takagi, R. Haruki and S.-I. Adachi, *Sci. Adv.*, 2018, **4**, eaat8466.
- [7] P. Jonkheijm, P. van der Schoot, A. P. H. J. Schenning and E. W. Meijer, *Science*, 2006, **313**, 80-83.
- [8] M. M. J. Smulders, M. M. L. Nieuwenhuizen, T. F. A. de Greef, P. van der Schoot, A. P. H. J. Schenning and E. W. Meijer, *Chem. Eur. J.*, 2010, **16**, 362-367.
- [9] A. J. Markvoort, H. M. ten Eikelder, P. A. Hilbers, T. F. de Greef and E. W. Meijer, *Nat. Commun.*, 2011, **2**, 509.
- [10] T. F. A. De Greef, M. M. J. Smulders, M. Wolffs, A. P. H. J. Schenning, R. P. Sijbesma and E. W. Meijer, *Chem. Rev.*, 2009, **109**, 5687-5754.
- [11] S. Dhiman, A. Sarkar and S. J. George, *RSC Adv.*, 2018, **8**, 18913-18925.
- [12] M. Wehner, M. I. S. Röhr, M. Bühler, V. Stepanenko, W. Wagner and F. Würthner, *J. Am. Chem. Soc.*, 2019, **141**, 6092-6107.
- [13] Kazuo Nakamoto, *Infrared and Raman Spectra of Inorganic and Coordination Compounds*, Part B, Applications in Coordination, Organometallic, and Bioinorganic Chemistry, 6th edn Wiley, 2009.
- [14] E. Espinosa, E. Molins and C. Lecomte, *Chem. Phys. Lett.*, 1998, **285**, 170-173.